

# Biomass burning at Cape Grim: exploring photochemistry using multi-scale modelling

S. J. Lawson<sup>1</sup>, M. Cope<sup>1</sup>, S. Lee<sup>1</sup>, I.E. Galbally<sup>1</sup>, Z. Ristovski<sup>2</sup> and M.D. Keywood<sup>1</sup>

[1] Commonwealth Scientific and Industrial Research Organisation, Climate Science Centre, Aspendale, Australia

[2] International Laboratory for Air Quality & Health, Queensland University of Technology, Brisbane, Australia

Correspondence to: S. J. Lawson (sarah.lawson@csiro.au)

## Abstract

We have tested the ability of a high resolution chemical transport model (CTM) to reproduce biomass burning (BB) plume strikes and ozone (O<sub>3</sub>) enhancements observed at Cape Grim in Tasmania Australia from the Robbins Island fire. The CTM has also been used to explore the contribution of near-field BB emissions and background sources to O<sub>3</sub> observations under conditions of complex meteorology. Using atmospheric observations, we have tested model sensitivity to meteorology, BB emission factors (EF) corresponding to low, medium and high modified combustion efficiency (MCE) and spatial variability. The use of two different meteorological models (TAPM-CTM and CCAM-CTM) varied the first (BB1) plume strike time by up to 15 hours, and duration of impact between 12 and 36 hours, and varied the second (BB2) plume duration between 50 and 57 hours. Meteorology also had a large impact on simulated O<sub>3</sub>, with one model (TAPM-CTM) simulating 4 periods of O<sub>3</sub> enhancement, while the other model (CCAM) simulating only one period. Varying the BB EFs, which in turn varied the non-methane organic compound (NMOC) / oxides of nitrogen (NO<sub>x</sub>) ratio, had a strongly non-linear impact on simulated O<sub>3</sub> concentration, with either destruction or production of O<sub>3</sub> predicted in different simulations. As shown in previous work (Lawson et al., 2015), minor rainfall events have the potential to significantly alter EF due to changes in combustion processes. Models which assume fixed EF for O<sub>3</sub> precursor species in an environment with temporally or spatially variable EF may be unable to simulate the behaviour of important species such as O<sub>3</sub>.

30 TAPM-CTM is used to further explore the contribution of the Robbins Island fire to the  
31 observed O<sub>3</sub> enhancements during BB1 and BB2. Overall, TAPM-CTM suggests the dominant  
32 source of O<sub>3</sub> observed at Cape Grim was aged urban air (age = 2 days), with a contribution of  
33 O<sub>3</sub> formed from local BB emissions.

34 This work shows the importance of assessing model sensitivity to meteorology and EF, and the  
35 large impact these variables can have in particular on simulated destruction or production of  
36 O<sub>3</sub> in regional atmospheric chemistry simulations.

37

## 38 **1 Introduction**

39 Biomass burning (BB) makes a major global contribution to atmospheric trace gases and  
40 particles with ramifications for human health, air quality and climate. Directly emitted species  
41 include carbon monoxide (CO), carbon dioxide (CO<sub>2</sub>), oxides of nitrogen (NO<sub>x</sub>), primary  
42 organic aerosol (POA), non-methane organic compounds (NMOC) and black carbon (BC),  
43 while chemical transformations occurring in the plume over time lead to formation of  
44 secondary species such as O<sub>3</sub>, oxygenated NMOC and secondary aerosol. Depending on a  
45 number of factors, including magnitude and duration of fire, plume rise and meteorology, the  
46 impact of BB plumes on human health, air quality and climate may be local, regional or global.

47 BB plumes from wildfires, prescribed burning, agricultural and trash burning can have a major  
48 impact on air quality in both urban and rural centres (Keywood et al., 2015; Luhar et al., 2008;  
49 Reisen et al., 2011; Emmons et al., 2010; Yokelson et al., 2011) and regional scale climate  
50 impacts (Andreae et al., 2002; Keywood et al., 2011b; Artaxo et al., 2013; Anderson et al.,  
51 2016). In Australia, BB from wild and prescribed fires impacts air quality in both rural and  
52 urban areas (Keywood et al., 2015; Reisen et al., 2011; Luhar et al., 2008; Keywood et al.,  
53 2011a) as well as indoor air quality (Reisen et al., 2011). More generally, as human population  
54 density increases, and as wildfires become more frequent (Flannigan et al., 2009; Keywood et  
55 al., 2011b), assessing the impact of BB on air quality and human health becomes more urgent  
56 (Keywood et al., 2011b; Reisen et al., 2015). In particular, particles emitted from BB frequently  
57 lead to exceedances of air quality standards, and exposure to BB particles has been linked to  
58 poor health outcomes including respiratory effects, cardiovascular disease and mortality  
59 (Reisen et al., 2015; Reid et al., 2016; Dennekamp et al., 2015). There is also increasing  
60 evidence that mixing of BB emissions with urban emissions results in enhanced  
61 photochemistry and production of secondary pollutants such as secondary aerosol and O<sub>3</sub> (Jaffe

62 and Wigder, 2012; Akagi et al., 2013; Hecobian et al., 2012), which may result in more  
63 significant health impacts than exposure to unmixed BB or urban emissions.

64 To be able to accurately predict and assess the impact of BB on human health, air quality and  
65 climate, models must be able to realistically simulate the chemical and microphysical processes  
66 that occur in a plume as well as plume transport and dispersion. In the case of BB plumes close  
67 to an urban centre or other sensitive receptor, models can be used to mitigate risks on  
68 community by forecasting where and when a BB plume will impact, the concentrations of toxic  
69 trace gases and particles in the plume, and potential impact of the BB plume mixing with other  
70 sources. Models also allow investigation of the contributions from BB and other sources on  
71 observed air quality when multiple sources are contributing. Understanding the relative  
72 importance of different sources is required when formulating policy decisions to improve air  
73 quality.

74 Lagrangian parcel models are often used to investigate photochemical transformations in BB  
75 plumes as they are transported and diluted downwind (Jost et al., 2003; Trentmann et al., 2005;  
76 Mason et al., 2006; Alvarado and Prinn, 2009; Alvarado et al., 2015) while three-dimensional  
77 (3D) Eulerian grid models have been used to investigate transport and dispersion of plumes,  
78 plume age, as well as contributions from different sources. 3D Eulerian grid models vary from  
79 fine spatial resolution on order of a few kilometers (Luhar et al., 2008; Keywood et al., 2015;  
80 Alvarado et al., 2009; Lei et al., 2013) to a resolution of up to hundreds of kilometers in global  
81 models (Arnold et al., 2015; Parrington et al., 2012).

82 Sensitivity studies have allowed the influence of different model components (emissions,  
83 plume rise, transport, chemistry) on model output to be investigated. Such studies are  
84 particularly important in formation of secondary species such as O<sub>3</sub> which have a non-linear  
85 relationship with emissions. Studies have found that modelled O<sub>3</sub> concentration from BB  
86 emissions is highly dependant on a range of factors including a) meteorology (plume transport  
87 and dispersion) in global (Arnold et al., 2015) and high resolution (Lei et al., 2013) Eulerian  
88 grid models, b) absolute emissions/biomass burned (Pacifico et al., 2015; Parrington et al.,  
89 2012), c) model grid size resulting in different degrees of plume dilution (Alvarado et al.,  
90 2009), and oxidative photochemical reaction mechanisms in Lagrangian parcel models (Mason  
91 et al., 2006).

92 Broadly speaking, models used for simulating BB plumes comprise a) description of the  
93 emissions source b) a determination of plume rise c) treatment of the vertical transport and

94 dispersion and d) a mechanism for simulating chemical transformations in the plume (Goodrick  
95 et al., 2013). There are challenges associated with accurately representing each of these  
96 components in BB modelling. The description of emissions source includes a spatial and  
97 temporal description of the area burnt, the fuel load, combustion completeness, and trace gas  
98 and aerosol emission factors (mass of species emitted per mass of fuel burned).. The area  
99 burned is often determined by a combination of hotspot and fire scar data, determined from  
100 retrievals from satellite (Kaiser et al., 2012; Reid et al., 2009(Giglio et al., 2013)). Cloud cover  
101 may lead to difficulties in obtaining area burnt data, while scars from small fires may be  
102 difficult to discern against complex terrain, and low intensity fires may not correspond with a  
103 detectable hotspot (Meyer et al., 2008). Emission factors are determined experimentally either  
104 by field or laboratory measurements, and are typically grouped by biome type. In some regions,  
105 such as SE Australia, biomes have been sparsely characterised (Lawson et al., 2015).  
106 Furthermore, models use biome-averaged EF which do not account for complex intra-biome  
107 variation in EF as a result of temporal and spatial differences in environmental variables. This  
108 includes factors such as impact of vegetation structure, monthly average rainfall (van Leeuwen  
109 and van der Werf, 2011) and the influence of short term rainfall events (Lawson et al., 2015).  
110 For example, EFs have been shown to vary significantly with fuel moisture which can vary  
111 seasonally (Korontzi et al., 2003; Urbanski, 2013). There may be significant spatial variability  
112 in emission factors within a biome (Castellanos et al., 2014); taken along with temporal  
113 variability, this has been shown to have a large impact on simulated concentrations of BB  
114 species in global-scale modelling (van Leeuwen et al., 2013).

115 Finally, the very complex mixture of trace gases and aerosols in BB plumes creates analytical  
116 challenges in quantifying EF, especially for semi and low volatility organics which are  
117 challenging to measure and identify but contribute significantly to secondary aerosol formation  
118 and photochemistry within the plume (Alvarado and Prinn, 2009; Alvarado et al., 2015; Ortega  
119 et al., 2013).

120 Plume rise is a description of how high the buoyant smoke plume rises above the fire, and  
121 consequently the initial vertical distribution of trace gases and aerosols in the plume (Freitas  
122 et al., 2007). This is still a large area of uncertainty in BB models, with a generalised plume  
123 rise approach typically used which may include either homogenous mixing, prescribed  
124 fractions of emissions distributed according to mixing height, use of parametisations, and  
125 finally plume rise calculated according to atmospheric dynamics. A key driver of this  
126 uncertainty is the complexity of fire behaviour resulting in high spatial and temporal

127 variability of pollutant and heat release, which drives variability in plume rise behaviour,  
128 such as multiple updraft cores (Goodrick et al., 2013).

129 Transport and dilution in models is driven by meteorology, particularly wind speed and  
130 direction, wind shear and atmospheric stability. Meteorology has a large impact on the ability  
131 of models to simulate the timing and magnitude and even composition of BB plume impacts in  
132 both local and regional scale models (Lei et al., 2013; Luhar et al., 2008; Arnold et al., 2015).  
133 For example, too-high wind speeds can lead to modelled pollutant levels which are lower than  
134 observed (e.g. Lei et al., 2013) while small deviations in wind direction lead to large  
135 concentration differences between modelled and observed, particularly when modelling  
136 emissions of multiple spatially diverse fires (Luhar et al., 2008). Dilution of BB emissions in  
137 large grid boxes in global models may also lead to discrepancies between modelled and  
138 observed  $\text{NO}_x$ ,  $\text{O}_3$  and aerosols (Alvarado et al., 2009).

139 Finally, models use a variety of gas-phase and aerosol-phase physical and chemical schemes,  
140 which vary in their ability to accurately represent chemical transformations, including  
141 formation of  $\text{O}_3$  and organic aerosol (Alvarado and Prinn, 2009; Alvarado et al., 2015).  
142 Validating and constraining chemical transformations in models requires high quality, high  
143 time resolution BB observations of a wide range of trace gas and aerosol species, including  
144 important but infrequently measured species such as OH and semi volatile and low volatility  
145 NMOC. Field observations, whilst often temporally and spatially scarce, are particularly  
146 valuable because the processes and products of BB plume processing are dependent on long  
147 range transport, cloud processing, varying meteorological conditions and heterogeneous  
148 reactions.

149 In this work we test the ability of CSIRO's high resolution 3D Eulerian grid chemical transport  
150 model (CTM) to reproduce BB plume observations of the Robbins Island fire reported in  
151 Lawson et al., (2015) with a focus on CO, BC and  $\text{O}_3$ . We undertake sensitivity studies using  
152 varying emission factors associated with a low, medium and high Modified Combustion  
153 Efficiency (MCE), which in turn changes the NMOC /  $\text{NO}_x$  ratio, in contrast to other sensitivity  
154 studies which typically vary emissions linearly. We also test sensitivity to meteorology by  
155 coupling the CTM with two different meteorological models, TAPM and CCAM. The fire and  
156 fixed observation site (Cape Grim) were only 20 km apart, and so simulation of the plume  
157 strikes is a stringent test of TAPM and CCAM's ability to reproduce windspeed and direction.  
158 Plume rise and chemical mechanism are held constant. Finally, we use TAPM-CTM to separate  
159 the contribution of the Robbins Island fire emissions and urban emissions to the observed  $\text{O}_3$

160 enhancements at Cape Grim reported in Lawson et al., (2015), and to determine the age of the  
161 O<sub>3</sub>-enhanced air parcels.

## 162 **2 Methods**

### 163 **2.1 Fire and measurement details**

164 Details of the fire and measurements are given in Lawson et al (2015). Briefly, biomass burning  
165 (BB) plumes were measured at the Cape Grim Baseline Air Pollution Station during the 2006  
166 Precursors to Particles campaign, when emissions from a fire on nearby Robbins Island  
167 impacted the station. Fire burned through native heathland and pasture grass on Robbins Island  
168 some 20 km to the east of Cape Grim for two weeks in February 2006. On two occasions an  
169 easterly wind advected the BB plume directly to the Cape Grim Station. The first plume strike  
170 (BB1) occurred from 02:00 – 06:00 (Australian Eastern Standard Time - AEST) on the 16th  
171 February, with light easterly winds of 3 m s<sup>-1</sup> and temperature of 13 °C and RH of 96 %. The  
172 second, more prolonged plume strike (BB2) occurred from 23:00 on 23rd February to 05:00  
173 on the 25th February, with strong easterly winds ranging from 10-16 m s<sup>-1</sup>, temperatures of 16-  
174 22 °C and RH in the range of 75-95 %. Under a northerly wind direction, urban air from the  
175 city of Melbourne (population 4.2 million) some 300 km away is transported across the ocean  
176 (Bass Strait) to Cape Grim.

177 A wide variety of trace gas and aerosol measurements were made during the fire event (Lawson  
178 et al., 2015). In this work, measurements of black carbon (BC), carbon monoxide (CO) and  
179 ozone (O<sub>3</sub>) are compared with model output. BC measurements were made using an  
180 aethelometer (Gras, 2007), CO measurements were made using an AGAGE gas  
181 chromatography system with a multi-detector (Krummel et al., 2007) and O<sub>3</sub> measurements  
182 were made using a TECO analyser (Galbally et al., 2007). For further details see Lawson et al.,  
183 (2015).

### 184 **2.2 Chemical transport models**

185 Simulations were undertaken with CSIRO's chemical transport model (CTM), coupled offline  
186 with two meteorological models (see below). The CSIRO CTM is a three-dimensional Eulerian  
187 chemical transport model with the capability of modelling the emission, transport, chemical  
188 transformation, wet and dry deposition of a coupled gas and aerosol phase atmospheric system.  
189 The CTM was initially developed for air quality forecasting (Cope et al., 2004) and has had

190 extensive use with shipping emission simulations (Broome et al., 2016), urban air quality (Cope  
191 et al., 2014; Galbally et al., 2008), biogenic (Emmerson et al., 2016) and biomass burning  
192 studies (Keywood et al., 2015; Meyer et al., 2008; Luhar et al., 2008).

193 The chemical transformation of gas-phase species was modelled using an extended version of  
194 the Carbon Bond 5 mechanism (Sarwar et al., 2008) with updated toluene chemistry (Sarwar  
195 et al., 2011). The mechanism was also extended to include the gas phase precursors for  
196 secondary (gas and aqueous phase) inorganic and organic aerosols. Secondary inorganic  
197 aerosols were assumed to exist in thermodynamic equilibrium with gas phase precursors and  
198 were modelled using the ISORROPIA-II model (Fountoukis and Nenes, 2007). Secondary  
199 organic aerosol (SOA) was modelled using the Volatility Basis Set (VBS) approach (Donahue  
200 et al., 2006). The VBS configuration is similar to that described in Tsimpidi et al., (2010). The  
201 production of S-VI in cloud water was modelled using the approach described in Seinfeld and  
202 Pandis (1998). The boundary concentrations in the models for different wind directions were  
203 informed by Cape Grim observations of atmospheric constituents during non BB periods  
204 (Lawson et al., 2015). In this work the modelled elemental carbon (EC) output was considered  
205 equivalent to the BC measured with aethalometer at Cape Grim.

206 Horizontal diffusion is simulated according to equations detailed in Cope et al (2009) according  
207 to principles of Smagorinsky et al., (1963) and Hess (1989). Vertical diffusion is simulated  
208 according to equations detailed in Cope et al., (2009) according to principles of Draxler and  
209 Hess (1997). Horizontal and vertical advection uses the approach of Walcek et al., (2000).

### 210 2.2.1 Meteorological models

211 Prognostic meteorological modelling was used for the prediction of meteorological fields  
212 including wind velocity, temperature, water vapour mixing ratio and clouds, radiation and  
213 turbulence. The meteorological fields force key components of the emissions and the chemical  
214 transport model. Two meteorological models were used in this work. CSIRO's (The) Air  
215 Pollution Model (TAPM) (Hurley, 2008b), a limited area, nest-able, three-dimensional  
216 Eulerian numerical weather and air quality prediction system, and CSIRO's Conformal Cubic  
217 Atmospheric Model (CCAM) a global stretched grid atmospheric simulation model  
218 (McGregor, (2015) and references therein). The models represent two unique (and  
219 independent) approaches for generating the meteorological fields required by the chemical  
220 transport model.

221 For CCAM, 20 km spaced simulations over Australia were used by the CTM (with the same  
222 grid spacing) to model large scale processes on the continent including the emission and  
223 transport of windblown dust, sea salt aerosol and smoke from wildfires. Note that the governing  
224 equations for TAPM do not enable this model to simulate spatial scales greater than 1000 km  
225 in the horizontal and thus only the CCAM meteorology was available for the continental-scale  
226 simulations. TAPM and CCAM 12 km spaced simulations were then used to model the  
227 transport of the Melbourne plume to Cape Grim by the CTM (at 12 km grid spacing) with  
228 boundary conditions provided by the continental simulation. Nested grid simulations by the  
229 CTM at 3 km and 1 km grid spacing utilised TAPM and CCAM meteorology simulated at  
230 matching grid spacing. The 1 km spaced meteorological fields were also used to drive a 400 m  
231 spaced CTM domain which encompassed Robbin's Island and Cape Grim. This domain was  
232 included in the nested grid system because we wanted to better numerically resolve the spatial  
233 extent of the fire and the process of plume advection between Robbin's Island and Cape Grim.  
234 In this work the CTM coupled with CCAM meteorological model is referred to as CTM-  
235 CCAM, while the CTM coupled with the TAPM meteorological model is referred to as TAPM-  
236 CTM.

## 237 2.2.2 Emission inventories

### 238 **Anthropogenic emissions**

239 Anthropogenic emissions for Victoria were based on the work of Delaney et al., (2011). No  
240 anthropogenic emissions were included for Tasmania. The north-west section of Tasmania has  
241 limited habitation and is mainly farmland, and so the influence of Tasmanian anthropogenic  
242 emissions on Cape Grim are expected to be negligible.

### 243 **Natural and Biogenic emissions**

244 The modelling framework includes methodologies for estimating emissions of sea salt aerosol  
245 (Gong, 2003) emissions of windblown dust (Lu and Shao, 1999); gaseous and aerosol  
246 emissions from managed and unmanaged wild fires (Meyer et al., 2008); emissions of NMOC  
247 from vegetation (Azzi et al., 2012) and emissions of nitric oxide and ammonia from vegetation  
248 and soils. Emissions from all but the wildfires are calculated inline in the CTM at each time  
249 step using the current meteorological fields. There were no other major fires burning in Victoria  
250 and Tasmania during the study period.

### 251 **Emissions – Robbins Island fire**



252 The area burnt by the fire was determined from hotspots from the Sentinel product  
253 (Geosciences Australia) which were derived from MODIS imagery. The hotspots were  
254 buffered to give polygon spots at a resolution of 400ha spot<sup>-1</sup>, then merged into a single  
255 polygon for each fire day (Meyer et al., 2008). The fire burnt 2000 ha over the two week  
256 period, and the direction of fire spread was unknown. As such, the fire scar was divided up  
257 into 250m grids and the hourly areas burnt calculated using a normalised version of the  
258 Macarthur Fire Danger Index (FDI) (Meyer et al., 2008). The models assumed that an equal  
259 proportion of each grid burned simultaneously over the two week period. The fuel density used  
260 was estimated to be 18.7 t C ha<sup>-1</sup>, based on mean mass loads of coarse and fine fuels taken from  
261 the biogeochemical production model (VAST 1.2, Barrett 2002) and converted into carbon  
262 mass (Meyer et al., 2008).

263 The hourly diurnal emissions of all gases and particles from the fire were calculated using the  
264 FDI in which the presence of strong winds will result in faster fire spread and enhanced  
265 emissions, compared to periods of lower wind speeds. The effect of wind speed on the fire  
266 behaviour and emissions is particularly important during the second BB event in which the  
267 winds ranged from 10 to 15 m s<sup>-1</sup>. This is evident from Figure 2 where hourly emission profiles  
268 based on an average diurnal FDI calculated by Meyer et al., (2008) (which peaks early  
269 afternoon) is compared with profiles based on hourly FDI generated by TAPM and CCAM  
270 meteorology. It can be seen that the use of the dynamic FDI approach during the BB2 period  
271 increases the Base emissions by 70% for TAPM meteorology and by 45% for the CCAM  
272 meteorology. It is also notable that the use of the dynamic approach with TAPM meteorology  
273 leads to the peak emissions occurring overnight on the 24<sup>th</sup> Feb which is when the Base  
274 emissions are at a minimum.

275 Savanna category EF were used as base case EFs in this work from Andreae and Merlet (2001).  
276 Three different sets of fire emission factors, corresponding to low, medium and high MCE  
277 were used to test the sensitivity of the models, where  $MCE = \Delta CO_2 / \Delta CO + \Delta CO_2$  (Ferek et  
278 al., 1998). We used published EF of CO and CO<sub>2</sub> from temperate forests (Akagi et al., 2011),  
279 to calculate a typical range of MCEs for temperate fires, including an average (best estimate)  
280 of 0.92, a lower (0.89) and upper estimate (0.95). Fires with MCEs of approximately 0.90  
281 consume biomass with approximately equal amounts of smouldering and flaming, while MCEs  
282 of 0.99 indicate complete flaming combustion (Akagi et al., 2011). Therefore the calculated  
283 range of MCEs (0.89 - 0.95) correspond to fires in which both smouldering and flaming is

284 occurring, with a tendency for more flaming combustion in the upper estimate (0.95) compared  
285 to a tendency of more smouldering in the lower estimate (0.89).

286 In previous smoke modelling work, CCAM-CTM and TAPM-CTM used savannah EF from  
287 Andreae and Merlet (2001). However, as Robbins Island is in a temperate region, the Andreae  
288 and Merlet (2001) savannah EF used in the models were adjusted to reflect temperate EF based  
289 on the following methodology. Minimum, mean and maximum CO EF for temperate forests  
290 from Agaki et al., (2011) were used for lower (0.89), best estimate (0.92) and upper MCE  
291 (0.95). For all other species, savannah EF (corresponding to MCE 0.94) were adjusted to EF  
292 for MCE=0.89, 0.92 and 0.95 using published relationships between MCE and EF (Meyer et  
293 al., 2012; Yokelson et al., 2007; Yokelson et al., 2003; Yokelson et al., 2011).

294 For example to adjust the Andreae and Merlet (2001) savannah EF (corresponding to an MCE  
295 of 0.94) to our temperate 'best estimate' EF (corresponding to MCE of 0.92) the Andreae and  
296 Merlet (2001) NO EF was reduced by 30%, the NMOC EFs were increased by 30%, the BC  
297 EF was reduced by 30% and the OC EF was increased by 20%. Table 1 gives emission factors  
298 for the original savannah EF (Andreae and Merlet, 2001) and the adjusted EF used in this work.  
299 The NO<sub>x</sub>/NMOC ratios used are also shown, and vary by a factor of 3 between the low and  
300 high MCE scenarios, mainly driven by the variability in NO emissions with MCE. The EF  
301 calculated from observations for this fire are shown for comparison (Lawson et al., 2015).

302 We recognise calculating EF in this way is approximate, however the purpose of including a  
303 range of EF was to explore the model's sensitivity to EF. While EFs were calculated for the  
304 Robbins Island fire for several species (Lawson et al., 2015), these are only available for a  
305 subset of species required by the CB05 chemical mechanism. The adjustment of the Andreae  
306 and Merlet (2001) Savannah EF to a lower MCE (0.89) resulted in good ( $\pm 20\%$ ) agreement  
307 with the calculated EF for CO, BC and several NMOC from Lawson et al., (2015), in which  
308 the MCE was calculated as 0.88. This provides confidence in using published relationships  
309 between MCE and EF to estimate EF in this work.

310 With respect to plume rise, the Robbin's Island fire was a relatively low energy burn (Lawson  
311 et al., 2015), and as noted by Paugam et al., (2016) the smoke from such fires is largely  
312 contained within the planetary boundary layer (PBL). Given that ground-based images of the  
313 Robbin's Island smoke plume support this hypothesis, in this work we adopted a simple  
314 approach of mixing the emitted smoke uniformly into the model's layers contained within the  
315 PBL. The plume was well mixed between the maximum of the PBL height and 200 m above

316 the ground, with the latter included to account for some vertical mixing of the buoyant smoke  
317 plume even under conditions of very low PBL height. The high wind speeds particularly during  
318 the second BB event, also suggest that the plume was not likely to be sufficiently buoyant to  
319 penetrate the PBL.

320

## 321 **3 Results and Discussion**

### 322 **3.1 Modelling Sensitivity Study**

323 The ability of the models to reproduce the two plume strikes (BB1 and BB2, described in  
324 Lawson et al (2015)) was tested. The period examined was the 13 February 2006 to the 28  
325 February 2006. The sensitivity of the models to meteorology, emission factors and spatial  
326 variability was also investigated and is discussed below. Observation and model data shown  
327 are hourly averages. Table 2 summarizes the main findings of the model sensitivity study. A  
328 MODIS Truecolour Aqua image of the Robbins Island fire plume is shown in Figure 3 from  
329 23 February 2006, with the modelled plume during the same period.

#### 330 **3.1.1 Sensitivity of modelled BB species to meteorology**

331 Qualitative and quantitative assessment of model performance for meteorological parameters  
332 were undertaken for both TAPM and CCAM. Hourly observed and modelled winds,  
333 temperature, humidity and PBL are compared and discussed in the Supplementary section  
334 (Figures S2-S8). Briefly, both TAPM and CCAM demonstrated reasonable skill in modelling  
335 the meteorological conditions, with the TAPM simulations slightly better than the CCAM with  
336 respect to the low level wind, temperatures and relative humidity and CCAM simulations  
337 slightly better in terms of PBL height.

#### 338 **Primary species- CO and BC**

339 Figure 4 and Figure 5 shows concentration isopleths generated by TAPM-CTM and CCAM-  
340 CTM respectively for BB1 with the models output every 12 hours shown. The narrow BB  
341 plume is simulated intermittently striking Cape Grim, and then the plume is swept away from  
342 Cape Grim after a wind direction change.

343 The simulated and observed time series concentrations of CO and BC for the two different  
344 models (TAPM-CTM and CCAM-CTM) and for 3 different sets of EF (discussed in Section  
345 3.1.2) are shown in Figure 6. TAPM-CTM and CCAM-CTM both reproduce the observed

346 plume strikes (BB1 and BB2). The impact of meteorology on the plume strike timing and  
347 duration is discussed below.

348 Both models overestimate the duration of BB1 and are a few hours out in the timing of the  
349 plume strike. TAPM-CTM predicts the timing of BB1 is 3 hours later than occurred (BC data)  
350 and predicts that BB1 persists for 12 hours (observed duration 5 hours) (Figure 4). CCAM-  
351 CTM predicts that BB1 occurs 12 hours prior to the observed plume strike and predicts that the  
352 plume intermittently sweeps across Cape Grim for up to 36 hours (Figure 5) . Both models  
353 indicate that the plume is narrow and meandering.

354 Both models overestimate the duration of BB2 and simulate the plume strike occurring earlier  
355 than observed. TAPM-CTM predicts BB2 is 26 hours earlier than observed and that BB2  
356 persists for 50 hours (observed duration 29 hours). CCAM-CTM predicts BB2 is 26 hours  
357 earlier than observed and that BB2 persists for 57 hours. It should be noted that there is a brief  
358 observed enhancement of BB species which correspond with the beginning of the modelled  
359 BB2 plume strike, some 24 hours prior to the prolonged observed event. This was likely due  
360 to the edge of the plume impacting the station briefly.

361

362 In both observed BB1 and BB2 the plume strike at Cape Grim occurred just prior to a wind  
363 direction change from easterly (fire direction), to south-westerly. The timing of the wind  
364 direction change in the models is therefore crucial to correctly predicting plume strike time and  
365 duration. In BB1 CCAM predicts an earlier wind direction change with higher windspeeds  
366 which advects the plume directly over Cape Grim while TAPM predicts a later wind change,  
367 lower windspeeds and advection of only the edge of the plume over Cape Grim. The higher  
368 concentrations CO and BC in BB1 by CCAM-CTM is are likely due to the direct advection of  
369 the plume over the site compared to only the plume edge in TAPM-CTM.

370 In BB2, both TAPM-CTM and CCAM-CTM predict direct strikes of the Robbin's Island  
371 smoke plume on Cape Grim, because the wind direction is modelled to be predominantly  
372 easterly for the duration of the event (Fig S18). Both models simulate some backing and  
373 veering of the wind direction for the duration of BB2 due to gravity waves processes which  
374 lead to intermittent strikes on Cape Grim as the Robbin's Island smoke plume sweeps to the  
375 north and south of Cape Grim. The gravity wave oscillations are more pronounced in CCAM-  
376 CTM than TAPM-CTM (and thus the plume strikes are more pronounced from the former) due

377 to differences in how the models are coupled to large scale synoptic forcing. The event is  
378 eventually curtailed by the passage of a south-westerly change.

379 Fig. S18 shows that TAPM-CTM predicts the onset of the change to occur about six hours  
380 ahead of the observed change and thus the BB2 event ends too early for this meteorological  
381 simulation. CCAM-CTM models the south-westerly change to occur one hour after the  
382 observed, leading to the modelled BB2 event extending beyond the observed duration for this  
383 meteorological simulation.

384 Differences in the magnitude of the modelled CO and BC peaks for TAPM-CTM and CCAM-  
385 CTM have two principal cause: a), the coupling of the smoke emissions to the TAPM and  
386 CCAM meteorology via the FDI scaling leads to approximately 20% higher emissions in the  
387 case of the TAPM-CTM simulations; b), the CCAM wind speeds are 20-50% higher than the  
388 TAPM wind speeds during BB2, which in combination with the emission differences, leads to  
389 TAPM-CTM generating near-surface smoke concentrations which are up to 80% higher than  
390 CCAM-CTM. Mixing depth can also play an important role in plume dispersion, however the  
391 PBL heights generated by both models are similar and generally low during BB2 due to the  
392 easterly wind direction and the mainly maritime upwind fetch.

### 393 **Secondary species – O<sub>3</sub>**

394 Figure 6 e-f shows the simulated and actual O<sub>3</sub> concentration time series for TAPM-CTM and  
395 CCAM-CTM for 3 different sets of EF (discussed in Section 3.1.2). The two observed O<sub>3</sub> peaks  
396 which followed BB1 and BB2 can clearly be seen in the time series of observations. Figure 7  
397 shows the TAPM-CTM and CCAM-CTM concentration isopleths of O<sub>3</sub> enhancement  
398 downwind of the fire during BB1 at 11:00 and 13:00 on the 16 February.

399 Again the simulated meteorology has a major impact on the ability of the models to reproduce  
400 the magnitude and timing of the observed O<sub>3</sub> peaks. TAPM-CTM reproduces the major O<sub>3</sub> peak  
401 observed following BB2, and captures part of the O<sub>3</sub> peak following BB1. For the peak  
402 following BB1 it under predicts the peak duration and fails to capture the subsequent observed  
403 peaks on the 19th and 19th February. TAPM-CTM also shows 2 additional O<sub>3</sub> peaks about  
404 24 hours prior to the BB1 and BB2 peaks respectively, which were not observed. The  
405 magnitude of these additional peaks shows a strong dependency on the EF suggesting an  
406 influence of fire emissions. This is discussed further below and in Section 3.2.1. Compared to  
407 TAPM-CTM, CCAM-CTM predicts fewer distinct peaks of ozone above the background  
408 (where background is 15-17 ppb) throughout the entire period. Both TAPM-CTM and CCAM-

409 CTM show depletion of O<sub>3</sub> below background levels which was not observed, and this is  
410 discussed further in Section 3.1.2.

411 Figure 7 shows that there are differences in wind fields between TAPM-CTM and CCAM-  
412 CTM as well as different simulated concentrations of O<sub>3</sub> generated from the fire. This is  
413 discussed further in Section 3.1.2. To summarise, the impact of using two different  
414 meteorological models for a primary species such as BC was to vary the modelled time of  
415 impact of the BB1 plume strike by up to 15 hours (CCAM-CTM -12 and TAPM-CTM +3  
416 hours, where actual plume strike time = 0 hours) and to vary the plume duration between 12  
417 and 36 hours (actual duration 5 hours). For BB2, different meteorological models predicted the  
418 same impact time (TAPM-CTM and CCAM-CTM both -26 hours where actual plume strike  
419 time = 0 hours) and to vary the plume duration between 47 and 60 hours (actual duration 29  
420 hours).

421 For O<sub>3</sub>, the use of different meteorological models lead to one model (TAPM-CTM)  
422 reproducing both observed peaks plus two additional peaks, while the other model (CCAM-  
423 CTM) captured only one defined O<sub>3</sub> peak over the time series of 2 weeks.

### 424 3.1.2 Sensitivity of modelled BB species to Emission Factors

#### 425 **Primary species – CO and BC**

426 Figure 6 a-d shows the simulated and observed concentrations of BC and CO for MCE=0.89,  
427 MCE=0.92 and MCE=0.95 (see Section 2.2.2). Because CO has a negative relationship with  
428 MCE, and BC has a positive relationship with MCE, the modelled BC concentrations are  
429 highest for model runs using the highest MCE, while the modelled CO concentrations are  
430 highest for model runs using the lowest MCE ( Figure 6).

431 Changing the EF from low to high MCE varies the modelled BC concentrations during BB1  
432 and BB2 by a factor of ~3 for BC and a factor of ~2 for CO, and increases the EF ratio of  
433 BC/CO by a factor of ~6, in proportion to the difference in EF input to the models.

434 Quantile-quantile plots of observed and modelled ratios of BC/CO during BB1 and BB2 for  
435 the different EF scenarios are shown in Fig S11. The use of BC/CO ratios were used to  
436 minimise uncertainty resulting from errors in modelling transport, dilution (and mixing height),  
437 thus enabling a focus on the impact of EF variability. A period incorporating both the modelled  
438 and observed BB1 and BB2 was used for the analysis. The TAPM-CTM simulation with  
439 MCE=0.89 performed best with greater than 60% of the model percentiles falling within a

440 factor of two of the observed. The CCAM-CTM simulation with MCE = 0.89 was the second  
441 best performer with 50% of the modelled percentiles falling within a factor of two of the  
442 observed. Overestimates of the EC/CO ratio by up to a factor of 8 occur for some percentiles  
443 for the MCE=0.95 scenarios, while the scenarios with no fire significantly underestimated the  
444 observed ratio. Plots of mean fractional bias and mean fractional error (Fig. S12 and S13) show  
445 that TAPM-CTM simulation with MCE=0.89 has the smallest bias and error, followed by the  
446 CCAM-CTM simulation with MCE=0.89. As discussed previously there is uncertainty in the  
447 derivation of EF as a function of MCE, as these were based on relationships from a small  
448 number of studies. Nevertheless, the percentile, bias and error analysis indicates that using  
449 emission factors corresponding to an MCE of 0.89 gives the best agreement with the  
450 observations for the BC/CO ratio. This is in agreement with the calculated MCE of 0.88 for  
451 this fire (Lawson et al., 2015)

452

453

#### 454 **Secondary species - O<sub>3</sub>**

455 For secondary species such as O<sub>3</sub> ( Figure 6e-f), the relationship between EF precursor gases  
456 and model output is more complex than for primary species such as CO and BC, because the  
457 balance between O<sub>3</sub> formation and destruction is dependent on the degree of dilution of the BB  
458 emissions and also factors such as the NMOC composition and the NMOC/NO<sub>x</sub> ratio.

459 TAPM-CTM ( Figure 6e) reproduces the magnitude of both observed peaks following BB1  
460 and BB2 (BB1 max observed = 33 ppb, modelled = 31 ppb, BB2 max observed = 34 ppb,  
461 modelled = 30ppb). Interestingly the magnitude of O<sub>3</sub> for these two peaks is the same for  
462 different EF inputs of O<sub>3</sub> precursors from the Robbins Island fire, suggesting that the BB  
463 emissions are not responsible for these enhancements as demonstrated in Section 3.2. In  
464 contrast, the two additional peaks modelled but not seen in the observations are heavily  
465 dependent on the input EF. For the first additional modelled peak which was predicted at the  
466 time of BB1 observations on the 16<sup>th</sup> February, all EF scenarios result in an O<sub>3</sub> peak, with the  
467 MCE=0.92 model scenario resulting in highest predicted O<sub>3</sub>. For the second additional  
468 modelled peak just prior to the BB2 observations on the 23<sup>rd</sup> February, only the MCE=0.89  
469 scenario results in a net O<sub>3</sub> production, while MCE=0.92 and MCE=0.95 scenarios lead to net  
470 O<sub>3</sub> destruction.

471 This differing response to EF for the TAPM-CTM runs suggests the importance of the NO EF  
472 on O<sub>3</sub> production in BB plumes. Unfortunately there were no oxides of nitrogen measurements  
473 made during the fire to test the models. For the first simulated additional peak prior to BB1,  
474 while the medium NO EF (MCE=0.92) resulted in the highest O<sub>3</sub> peak (with corresponding  
475 NO of 3.7 ppb, NO<sub>2</sub> 4.5 ppb) the lower NO EF in the 0.89 MCE run perhaps indicates  
476 insufficient NO was present to drive O<sub>3</sub> production (corresponding NO 0.5 ppb, NO<sub>2</sub> 1.5 ppb),  
477 which is in line with studies which have shown that BB plumes are generally NO<sub>x</sub> limited  
478 (Akagi et al., 2013; Jaffe and Wigder, 2012; Wigder et al., 2013). Conversely the highest input  
479 NO EF (MCE=0.95) lead to net destruction of O<sub>3</sub> (NO 9 ppb, NO<sub>2</sub> 7 ppb), which is due to  
480 titration of O<sub>3</sub> with the larger amounts of NO emitted from the fire in these runs as indicated  
481 by excess NO (NO/NO<sub>2</sub> ratio > 1) at Cape Grim (where NO has a positive relationship with  
482 MCE). For the second additional peak prior to BB2, only the lowest NO EF run (MCE=0.89)  
483 resulted in net production of O<sub>3</sub> (NO 1.5 ppb NO<sub>2</sub> 2.6 ppb) in the medium and high MCE runs  
484 the background O<sub>3</sub> concentration is completely titrated (0 ppb) with NO concentrations of 10  
485 and 20 ppb and NO/NO<sub>2</sub> ratios of 1.3 and 2.6 respectively.

486 In contrast, the CCAM-CTM model ( Figure 6f) simulations reproduce only the first observed  
487 O<sub>3</sub> peak associated with BB1 (modelled = 27 ppb, measured = 34 ppb). This modelled O<sub>3</sub> peak  
488 does not show an influence of MCE on O<sub>3</sub> concentration, in agreement with TAPM, again  
489 suggesting no influence from fire emissions as later demonstrated in Section 3.2. The CCAM  
490 model runs also show significant titration of O<sub>3</sub> during BB1 and BB2 for the medium and high  
491 MCE model runs, with ~24 and ~48 hours of significant O<sub>3</sub> depletion below background  
492 concentrations being modelled for each event, which was not observed

493 Quantile-quantile plots of modelled and observed concentrations of O<sub>3</sub> for all EF scenarios are  
494 shown in Fig. S14 and S15. Model performance was assessed for both the BB and the  
495 background periods in order to test the ability of the models to reproduce O<sub>3</sub> from both the fire  
496 and other sources, including urban sources. The modelled O<sub>3</sub> concentrations from the TAPM-  
497 CTM simulation with MCE=0.89 are close to the 1:1 line with observations for all of the  
498 sampled percentiles, and demonstrates that this scenario is in best agreement with observations,  
499 and as stated previously, in agreement with the calculated MCE of 0.88 for BB2 (Lawson et  
500 al., 2015). Ozone titration in the MCE=0.92 and MCE=0.95 scenarios, which was not observed,  
501 is visible as a significant deviation from the 1:1 line in Fig S14. With the exception of these  
502 titration events, all of the sampled model concentration percentiles fall well within a factor of  
503 two of the observations. Plots of mean fractional error and mean fractional bias (Figs S16 and



504 S17) show that the error and bias are very low for all runs and fall within performance  
505 guidelines.

506 The different EF scenarios presented here suggest that varying model EF has a major impact  
507 on whether the models simulate production or destruction of O<sub>3</sub>, particularly important at a  
508 receptor site in close proximity to the BB emissions. In the previous work (Lawson et al., 2015),  
509 the MCE for the first 10 hours of BB2 was calculated as 0.88, however later in BB2, a rainfall  
510 event led to changes in the NMOC/CO and BC/CO ratios. This suggests that during the course  
511 of BB2 the MCE decreased and thus EFs changed. As such, the used of fixed BB EF in this  
512 work and in other models, may lead to incorrect prediction of important species such as O<sub>3</sub>.”

### 513 3.1.3 Sensitivity of modelled concentrations to spatial variability

514 The near-field proximity of the Robbins Island fire (20 km) to Cape Grim, the narrowness of  
515 the BB plume and the spatial complexity of the modelled wind fields around north Tasmania  
516 are likely to result in strong heterogeneity in the modelled concentrations surrounding Cape  
517 Grim. We investigated how much model spatial gradients vary by sampling TAPM-CTM  
518 output with MCE=0.89 at 4 grid points sited 1 km to the north, east, south and west of Cape  
519 Grim.

#### 520 **Primary species - CO**

521 a shows a time series of the modelled CO output of the difference between Cape Grim and  
522 each grid point 1km either side.

523 Where plotted CO concentration is other location [CO] (N,S,E,W) –Cape Grim [CO].

524 The figure clearly shows that there are some large differences in the modelled concentrations  
525 of CO between grid points for both BB1 and BB2. Particularly large differences were seen for  
526 BB2 with the north gridpoint modelled concentrations in BB2 over 500 ppb lower than at Cape  
527 Grim grid point, while at the Southerly grid point the modelled CO was up to 350 ppb higher.  
528 Smaller differences of up to 250 ppb between the east and Cape Grim grid points were observed  
529 for BB1. This indicates the plume from the fire was narrow and had a highly variably impact  
530 on the area immediately surrounding Cape Grim.

531 Figure 8b shows the observed cumulative concentration of CO over the 29 hour duration of  
532 BB2 at Cape Grim, as well as the modelled cumulative concentration at Cape Grim and at the  
533 four gridpoints either side. This figure shows both the variability in concentration with location,  
534 but also with time. TAPM-CTM’s underestimation of the observed CO by is visible by hour

535 20. TAPM-CTM begins to show differences in modelled cumulative CO concentrations  
536 between the 5 gridpoints (including Cape Grim) by hour 10. At the end of BB2 TAPM-CTM  
537 predicts that there are differences of 5 - 30% between the cumulative modelled CO  
538 concentration at Cape Grim and the gridpoints to the north, east, south and west. This variability  
539 modelled between sites which are closely located highlights the challenges with modelling the  
540 impact of a near field fire at a fixed single point location. This also highlights the high spatial  
541 variability which may be missed in similar situations by using a coarser resolution model which  
542 would dilute emissions in a larger gridbox.

#### 543 **Ozone (O<sub>3</sub>)**

544 Figure 8c shows a time series of the modelled O<sub>3</sub> output of the difference between Cape Grim  
545 and each gridpoint 1km either side, where plotted O<sub>3</sub> concentration is other location [O<sub>3</sub>]  
546 (N,S,E,W) – Cape Grim [O<sub>3</sub>].

547 The modelled TAPM-CTM concentrations are very similar at all grid points when BB  
548 emissions are not impacting. The variability increases at the time of BB1 and BB2, with  
549 differences mostly within 2-3 ppb, but up to 15 and 10 ppb at east and west sites for BB1. This  
550 largest difference corresponds to the additional modelled O<sub>3</sub> peak which was not observed  
551 which showed strong dependency on EF (see Section 3.1.2), and provides further evidence that  
552 local BB emissions are driving this enhancement.

553 The TAPM-CTM output for O<sub>3</sub> for BB1(Figure 7) shows O<sub>3</sub> enhancement downwind of the  
554 fire at 11:00 and 13:00 on the 16 February. The very localised and narrow O<sub>3</sub> plume is dispersed  
555 by the light (2 m s<sup>-1</sup>) and variable winds, and Cape Grim is on the edge of the O<sub>3</sub> plume for  
556 much of this period, explaining the high variability seen in Figure 6c.

557 In summary there is a large amount of spatial variability in TAPM-CTM for primary species  
558 such as CO during the BB events, with differences of > 500 ppb in grid points 1 km apart. This  
559 is due to the close proximity of the fire to the observation site and narrow plume non-stationary  
560 meteorology. For O<sub>3</sub>, there is up to 15 ppb difference between grid points for a narrow O<sub>3</sub>  
561 plume which is formed downwind of the fire.

562 The highly localised nature of the primary and in some cases secondary species seen here  
563 highlights the benefits of assessing spatial variability in situations with a close proximity point  
564 source and a fixed receptor (measurement) site.

## 565 3.2 Exploring plume chemistry and contribution from different sources

### 566 3.2.1 Drivers of O<sub>3</sub> production

567 In previous work on the Robbins Island fire, it was noted that the increases in O<sub>3</sub> observed after  
568 both BB1 and BB2 were correlated with increased concentration of HFC134a (Lawson et al.,  
569 2015). This indicated that transport of photochemically processed air from urban areas to Cape  
570 Grim was likely the main driver of the O<sub>3</sub> observed, rather than BB emissions (Lawson et al.,  
571 2015). However, during BB1 in a calm sunny period with minimal urban influence, an increase  
572 in O<sub>3</sub> was observed alongside a period of particle growth and elevated BC, suggesting possible  
573 biomass burning influence. Normalised Excess Mixing Ratios (NEMR) observed during BB2  
574 were also in the range of those observed elsewhere in young BB plumes (Lawson et al., 2015)  
575 (where NEMR is an excess mixing ratio normalised to a non-reactive co-emitted tracer, in this  
576 case CO, see Akagi et al., 2011).

577 To explore this further, TAPM-CTM was used to determine the degree to which the local fire  
578 emissions, and urban emissions from mainland Australia, were driving the observed O<sub>3</sub>  
579 enhancements. The scenario with EF corresponding to MCE=0.89 was used, as discussed  
580 previously

581 Figure 9 shows the simulated ozone for all sources (With BB) and all sources excluding the  
582 Robbins Island fire (No BB). There are two additional distinct ozone peaks in the ‘With BB’  
583 simulation (Figure 9). These occurred during, or close to the plume strikes, and are short lived  
584 (3 and 5 hour) events. These same two peaks showed a strong dependence on model EF in  
585 Section 3.1.2. In contrast, the two peaks attributed to transport of air from mainland Australia  
586 are of longer duration, and occur after the plume strikes.

587 Of the 2 modelled fire-derived O<sub>3</sub> peaks, the first modelled peak (33 ppb) corresponds with a  
588 small (21 ppb) observed peak during BB1 (Period B in Lawson et al., 2015), but the second  
589 modelled fire-derived O<sub>3</sub> peak is not observed. As shown in Figure 7 and discussed in Section  
590 3.1.3, according to TAPM-CTM the O<sub>3</sub> plumes generated from fire emissions were narrow and  
591 showed a strong spatial variability. Given this, it is challenging for TAPM-CTM to predict the  
592 exact timing and magnitude of these highly variable BB generated O<sub>3</sub> peaks impacting Cape  
593 Grim. This is likely why there is good agreement in timing and magnitude between model and  
594 observations for the large scale, spatially homogeneous O<sub>3</sub> plumes transported from mainland  
595 Australia, but a lesser agreement for the locally formed, spatially variable O<sub>3</sub> formed from local  
596 fire emissions.

597 In summary, TAPM-CTM suggests that the the two largest observed O<sub>3</sub> peaks following BB1  
598 and BB2 were urban air transported from mainland Australia, and suggests some O<sub>3</sub> formation  
599 was driven by emissions from the local fire event. TAPM-CTM captures the magnitude and  
600 timing of the larger scale urban-derived peaks well, but is challenged by the timing and  
601 magnitude of O<sub>3</sub> from local BB emissions.

602

### 603 3.2.2 Plume age

604 TAPM-CTM was used to estimate the physical age of air parcels reaching Cape Grim over the  
605 two week period of the Robbins Island fire. The method is similar to the Eulerian effective  
606 physical age of emissions metric, accounting for mixing and chemical decay from Finch et al  
607 (2014) and has been described previously in Keywood et al., (2015). Briefly, two model  
608 simulations were run for scenarios which included all sources of nitric oxide (NO) in Australia  
609 ; the first treated NO as an unreactive tracer, the second with NO decaying at a constant first  
610 order rate. The relative fraction of the emitted NO molecules remaining after 96 hours was then  
611 inverted to give a molar-weighted plume age. As urban emissions are a larger NO source than  
612 BB, this approach would weight the age in the favour of the urban emissions if air masses from  
613 these two sources were mixed. However as shown in Figure 9, there are distinct periods where  
614 BB or urban sources dominate. As there is little mixing of air from the two sources, there are  
615 unlikely to be issues with the calculated age being weighted towards one source. Figure 10  
616 shows a time series of the modelled NO tracer (decayed version), modelled plume age (hours)  
617 and the observed O<sub>3</sub>. Direct BB1 and BB2 plume strikes can be clearly seen with increases in  
618 NO corresponding with a plume age of 0-2 hours. The plume age then gradually increases over  
619 24 hours in both cases, peaking at 15:00 on the 17th February during BB1 (aged of plume 40  
620 hours) and peaking at 17:00 on the 25th February during BB2 (age of plume 49 hours). The  
621 peak observed O<sub>3</sub> enhancements correspond with the simulated plume age in both BB1 and  
622 BB2 (with an offset of 2 hours for BB1), and the observed HFC-134a, suggesting that the plume  
623 which transported O<sub>3</sub> from Mebourne to Cape Grim was approximately 2 days old. TAPM-  
624 CTM also simulates a smaller NO peak alongside the maximum plume age, indicating transport  
625 of decayed NO from the mainland to Cape Grim.

626 As reported in Lawson et al., (2015), during BB2 NEMRs of  $\Delta O_3/\Delta CO$  ranged from 0.001-  
627 0.074, in agreement with O<sub>3</sub> enhancements observed in young BB plumes elsewhere (Yokelson  
628 et al., 2003; Yokelson et al., 2009). However, the modelling reported here suggests that almost

629 all of the O<sub>3</sub> observed during BB2 was of urban, not BB origin. This suggests NEMRs should  
630 not be used in isolation to identify the source of observed O<sub>3</sub> enhancements, and highlights the  
631 value of utilising air mass back trajectories and modelling to interpret the source of O<sub>3</sub>  
632 enhancements where there are multiple emission sources.

#### 633 **4 Summary and conclusions**

634 In this work we have used a unique set of opportunistic BB observations at Cape Grim Baseline  
635 Air Pollution Station to test the ability of CSIRO's high resolution (400m grid cell) CTM to  
636 reproduce primary (CO, BC) and secondary (O<sub>3</sub>) BB species in challenging non-stationary,  
637 inhomogeneous, and near field conditions. We tested the sensitivity of the CTM to three  
638 different parameters (meteorology, MCE and spatial variability) while holding the plume rise  
639 and the chemical mechanisms constant.

640 We found meteorology, EF and spatial variability have a large influence on the modelled output  
641 mainly due to the close proximity of the fire to the receptor site (Cape Grim). The lower MCE  
642 (MCE=0.89) TAPM-CTM model simulation provided the best agreement with the observed  
643 concentrations, in agreement with the MCE calculated from observations of 0.88 (Lawson et  
644 al., 2015). The changing EFs, in particular NO dependency on MCE, had a major influence on  
645 the simulated O<sub>3</sub> concentrations, with a tendency of the models in some configurations to both  
646 fail to simulate observed O<sub>3</sub> peaks, and to simulate complete titration of O<sub>3</sub> which was not  
647 observed. As shown in the previous work (Lawson et al., 2015), minor rainfall events have the  
648 potential to significantly alter EF due to changes in combustion processes. This work suggests  
649 that varying model EF has a major impact on whether the models predict production or  
650 destruction of O<sub>3</sub>, particularly important at a receptor site in close proximity to the BB  
651 emissions. Models which assume a fixed EF for O<sub>3</sub> precursor species in an environment with  
652 temporally and spatially variable EF may therefore be challenged to correctly predict the  
653 behaviour of important species such as O<sub>3</sub>.

654 There were significant differences in model output between Cape Grim and grid points 1 km  
655 away highlighting the narrowness of the plume and the challenge of predicting when the plume  
656 would impact the station. This also highlights the high spatial variability which may be missed  
657 in similar situations by using a coarser resolution model which would dilute emissions in a  
658 larger gridbox.

659 TAPM-CTM was used to distinguish the influence of the two sources on the observed O<sub>3</sub>  
660 enhancements which followed BB1 and BB2. Transport of a 2 day old urban plume some

661 300km away from Melbourne was the main source of the O<sub>3</sub> enhancement observed at Cape  
662 Grim over the two week period of the fire. Despite NEMRs of  $\Delta\text{O}_3/\Delta\text{CO}$  during BB2 being  
663 similar to that observed in young BB plumes elsewhere, this work suggests NEMRs should not  
664 be used in isolation to identify the source of observed O<sub>3</sub> enhancements, and highlights the  
665 value of utilising air mass back trajectories and modelling to interpret the source of O<sub>3</sub>  
666 enhancements where there are multiple emission sources.

667

## 668 **Acknowledgements**

669 The Cape Grim program, established by the Australian Government to monitor and study  
670 global atmospheric composition, is a joint responsibility of the Bureau of Meteorology  
671 (BOM) and the Commonwealth Scientific and Industrial Research Organisation (CSIRO).  
672 We thank the staff at Cape Grim and staff at CSIRO Oceans and Atmosphere for providing  
673 observation data for this work. Thank you to Nada Derek for producing figures, Mick Meyer  
674 for providing fire scar information, and Suzie Molloy for providing advice on ozone  
675 observation data. Finally we thank the three anonymous reviewers for their helpful  
676 suggestions and comments

677

## 678 **References**

679 **Akagi, S. K., Yokelson, R. J., Wiedinmyer, C., Alvarado, M. J., Reid, J. S., Karl, T.,**  
680 **Crouse, J. D., and Wennberg, P. O.: Emission factors for open and domestic biomass**  
681 **burning for use in atmospheric models, *Atmospheric Chemistry and Physics*, 11, 4039-**  
682 **4072, 10.5194/acp-11-4039-2011, 2011.**

683 **Akagi, S. K., Yokelson, R. J., Burling, I. R., Meinardi, S., Simpson, I., Blake, D. R.,**  
684 **McMeeking, G. R., Sullivan, A., Lee, T., Kreidenweis, S., Urbanski, S., Reardon, J.,**  
685 **Griffith, D. W. T., Johnson, T. J., and Weise, D. R.: Measurements of reactive trace gases**  
686 **and variable O<sub>3</sub> formation rates in some South Carolina biomass burning plumes, *Atmos.***  
687 ***Chem. Phys.*, 13, 1141-1165, 10.5194/acp-13-1141-2013, 2013.**

688 **Alvarado, M. J., and Prinn, R. G.: Formation of ozone and growth of aerosols in young**  
689 **smoke plumes from biomass burning: 1. Lagrangian parcel studies, *Journal of***  
690 ***Geophysical Research*, 114, 10.1029/2008jd011144, 2009.**

691 **Alvarado, M. J., Wang, C., and Prinn, R. G.: Formation of ozone and growth of aerosols**  
692 **in young smoke plumes from biomass burning: 2. Three-dimensional Eulerian studies,**  
693 ***Journal of Geophysical Research*, 114, 10.1029/2008jd011186, 2009.**

694 **Alvarado, M. J., Lonsdale, C. R., Yokelson, R. J., Akagi, S. K., Coe, H., Craven, J. S.,**  
695 **Fischer, E. V., McMeeking, G. R., Seinfeld, J. H., Soni, T., Taylor, J. W., Weise, D. R.,**  
696 **and Wold, C. E.: Investigating the links between ozone and organic aerosol chemistry in**

697 a biomass burning plume from a prescribed fire in California chaparral, *Atmos. Chem.*  
698 *Phys.*, **15**, 6667-6688, 10.5194/acp-15-6667-2015, 2015.

699 Anderson, D. C., Nicely, J. M., Salawitch, R. J., Canty, T. P., Dickerson, R. R., Hanisco,  
700 T. F., Wolfe, G. M., Apel, E. C., Atlas, E., Bannan, T., Bauguitte, S., Blake, N. J., Bresch,  
701 J. F., Campos, T. L., Carpenter, L. J., Cohen, M. D., Evans, M., Fernandez, R. P., Kahn,  
702 B. H., Kinnison, D. E., Hall, S. R., Harris, N. R., Hornbrook, R. S., Lamarque, J. F., Le  
703 Breton, M., Lee, J. D., Percival, C., Pfister, L., Pierce, R. B., Riemer, D. D., Saiz-Lopez,  
704 A., Stunder, B. J., Thompson, A. M., Ullmann, K., Vaughan, A., and Weinheimer, A. J.:  
705 A pervasive role for biomass burning in tropical high ozone/low water structures, *Nature*  
706 *communications*, **7**, 10267, 10.1038/ncomms10267, 2016.

707 Andreae, M. O., and Merlet, P.: Emission of trace gases and aerosols from biomass  
708 burning, *Global Biogeochemical Cycles*, **15**, 955-966, 10.1029/2000gb001382, 2001.

709 Andreae, M. O., Artaxo, P., Brandao, C., Carswell, F. E., Ciccioli, P., da Costa, A. L.,  
710 Culf, A. D., Esteves, J. L., Gash, J. H. C., Grace, J., Kabat, P., Lelieveld, J., Malhi, Y.,  
711 Manzi, A. O., Meixner, F. X., Nobre, A. D., Nobre, C., Ruivo, M., Silva-Dias, M. A.,  
712 Stefani, P., Valentini, R., von Jouanne, J., and Waterloo, M. J.: Biogeochemical cycling  
713 of carbon, water, energy, trace gases, and aerosols in Amazonia: The LBA-EUSTACH  
714 experiments, *Journal of Geophysical Research-Atmospheres*, **107**, 8066  
715 10.1029/2001jd000524, 2002.

716 Arnold, S. R., Emmons, L. K., Monks, S. A., Law, K. S., Ridley, D. A., Turquety, S.,  
717 Tilmes, S., Thomas, J. L., Bouarar, I., Flemming, J., Huijnen, V., Mao, J., Duncan, B. N.,  
718 Steenrod, S., Yoshida, Y., Langner, J., and Long, Y.: Biomass burning influence on high-  
719 latitude tropospheric ozone and reactive nitrogen in summer 2008: a multi-model  
720 analysis based on POLMIP simulations, *Atmospheric Chemistry and Physics*, **15**, 6047-  
721 6068, 10.5194/acp-15-6047-2015, 2015.

722 Artaxo, P., Rizzo, L. V., Brito, J. F., Barbosa, H. M. J., Arana, A., Sena, E. T., Cirino, G.  
723 G., Bastos, W., Martin, S. T., and Andreae, M. O.: Atmospheric aerosols in Amazonia  
724 and land use change: from natural biogenic to biomass burning conditions, *Faraday*  
725 *Discuss.*, **165**, 203-235, 10.1039/c3fd00052d, 2013.

726 Azzi, M., Cope, M., and Rae, M.: Sustainable Energy Deployment within the Greater  
727 Metropolitan Region. NSW- Environmental Trust 2012.

728 Barrett, D. J.: Steady state turnover time of carbon in the Australian terrestrial  
729 biosphere, *Global Biogeochemical Cycles*, **16**, 55-51-55-21, 10.1029/2002gb001860, 2002.

730 Broome, R. A., Cope, M. E., Goldsworthy, B., Goldsworthy, L., Emmerson, K., Jegasothy,  
731 E., and Morgan, G. G.: The mortality effect of ship-related fine particulate matter in the  
732 Sydney greater metropolitan region of NSW, Australia, *Environment International*, **87**,  
733 85-93, <http://dx.doi.org/10.1016/j.envint.2015.11.012>, 2016.

734 Castellanos, P., Boersma, K. F., and van der Werf, G. R.: Satellite observations indicate  
735 substantial spatiotemporal variability in biomass burning NO<sub>x</sub> emission factors for South  
736 America, *Atmospheric Chemistry and Physics*, **14**, 3929-3943, 10.5194/acp-14-3929-2014,  
737 2014.

738 Cope, M., Lee, S., Noonan, J., Lilley, B., Hess, G. D., and Azzi, M.: Chemical Transport  
739 Model - Technical Description, 2009.

740 Cope, M., Keywood, M., Emmerson, K., Galbally, I. E., Boast, K., Chambers, S., Cheng,  
741 M., Crumeyrolle, S., Dunne, E., Fedele, R., Gillett, R., Griffiths, A., Harnwell, J., Katzfey,

742 J., Hess, D., Lawson, S. J., Miljevic, B., Molloy, S., Powell, J., Reisen, F., Ristovski, Z.,  
743 Selleck, P., Ward, J., Zhang, C., and Zeng, J.: Sydney Particle Study Stage II., 2014.  
744 <http://141.243.32.146/resources/aqms/SydParticleStudy10-13.pdf>

745 Cope, M. E., Hess, G. D., Lee, S., Tory, K., Azzi, M., Carras, J., Lilley, W., Manins, P. C.,  
746 Nelson, P., Ng, L., Puri, K., Wong, N., Walsh, S., and Young, M.: The Australian Air  
747 Quality Forecasting System. Part I: Project Description and Early Outcomes, *Journal of*  
748 *Applied Meteorology*, **43**, 649-662, doi:10.1175/2093.1, 2004.

749 Delaney, W., and Marshall, A. G.: Victorian Air Emissions Inventory for 2006, 20th  
750 International Clean Air and Environment Conference, Auckland,, 2011.

751 Dennekamp, M., Straney, L. D., Erbas, B., Abramson, M. J., Keywood, M., Smith, K.,  
752 Sim, M. R., Glass, D. C., Del Monaco, A., Haikerwal, A., and Tonkin, A. M.: Forest Fire  
753 Smoke Exposures and Out-of-Hospital Cardiac Arrests in Melbourne, Australia: A Case-  
754 Crossover Study, *Environmental health perspectives*, **123**, 959-964, 10.1289/ehp.1408436,  
755 2015.

756 Donahue, N. M., Robinson, A. L., Stanier, C. O., and Pandis, S. N.: Coupled Partitioning,  
757 Dilution, and Chemical Aging of Semivolatile Organics, *Environmental Science &*  
758 *Technology*, **40**, 2635-2643, 10.1021/es052297c, 2006.

759 Draxler, R.R and Hess, G.D. .: Description of the HYSPLIT\_4 modeling system. NOAA  
760 Technical Memorandum ERL ARL-224, Air Resources Laboratory Silver Spring,  
761 Maryland, USA, 1997.

762 Emmerson, K. M., Galbally, I. E., Guenther, A. B., Paton-Walsh, C., Guerette, E. A.,  
763 Cope, M. E., Keywood, M. D., Lawson, S. J., Molloy, S. B., Dunne, E., Thatcher, M., Karl,  
764 T., and Maleknia, S. D.: Current estimates of biogenic emissions from eucalypts uncertain  
765 for southeast Australia, *Atmos. Chem. Phys.*, **16**, 6997-7011, 10.5194/acp-16-6997-2016,  
766 2016.

767 Emmons, L. K., Apel, E. C., Lamarque, J. F., Hess, P. G., Avery, M., Blake, D., Brune,  
768 W., Campos, T., Crawford, J., DeCarlo, P. F., Hall, S., Heikes, B., Holloway, J., Jimenez,  
769 J. L., Knapp, D. J., Kok, G., Mena-Carrasco, M., Olson, J., O'Sullivan, D., Sachse, G.,  
770 Walega, J., Weibring, P., Weinheimer, A., and Wiedinmyer, C.: Impact of Mexico City  
771 emissions on regional air quality from MOZART-4 simulations, *Atmospheric Chemistry*  
772 *and Physics*, **10**, 6195-6212, 10.5194/acp-10-6195-2010, 2010.

773 Finch, D. P., Palmer, P. I., and Parrington, M.: Origin, variability and age of biomass  
774 burning plumes intercepted during BORTAS-B, *Atmos. Chem. Phys.*, **14**, 13789-13800,  
775 10.5194/acp-14-13789-2014, 2014.

776 Ferek, R. J., Reid, J. S., Hobbs, P. V., Blake, D. R., and Liousse, C.: Emission factors of  
777 hydrocarbons, halocarbons, trace gases and particles from biomass burning in Brazil,  
778 *Journal of Geophysical Research: Atmospheres*, **103**, 32107-32118, 10.1029/98JD00692,  
779 1998.

780 Flannigan, M. D., Krawchuk, M. A., de Groot, W. J., Wotton, B. M., and Gowman, L.  
781 M.: Implications of changing climate for global wildland fire, *International Journal of*  
782 *Wildland Fire*, **18**, 483-507, <http://dx.doi.org/10.1071/WF08187>, 2009.

783 Fountoukis, C., and Nenes, A.: ISORROPIA II: a computationally efficient  
784 thermodynamic equilibrium model for K<sup>+</sup>-Ca<sup>2+</sup>-Mg<sup>2+</sup>-NH<sub>4</sub><sup>(+)</sup>-Na<sup>+</sup>-SO<sub>4</sub><sup>2-</sup>-NO<sub>3</sub><sup>-</sup>-Cl<sup>-</sup>-  
785 H<sub>2</sub>O aerosols, *Atmos Chem Phys*, **7**, 4639-4659, 2007.



786 Freitas, S. R., Longo, K. M., Chatfield, R., Latham, D., Silva Dias, M. A. F., Andreae, M.  
787 O., Prins, E., Santos, J. C., Gielow, R., and Carvalho Jr, J. A.: Including the sub-grid  
788 scale plume rise of vegetation fires in low resolution atmospheric transport models,  
789 *Atmos. Chem. Phys.*, 7, 3385-3398, 10.5194/acp-7-3385-2007, 2007.

790 Galbally, I. E., Cope, M., Lawson, S. J., Bentley, S. T., Cheng, M., Gillet, R. W., Selleck,  
791 P., Petraitis, B., Dunne, E., and Lee, S.: Sources of Ozone Precursors and Atmospheric  
792 Chemistry in a Typical Australian City, 2008.  
793 <http://olr.npi.gov.au/atmosphere/airquality/publications/pubs/ozone-precursors.pdf>

794 Galbally, I. E., Meyer, C. P., Bentley, S. T., Lawson, S. J., and Baly, S. B.: Reactive gases  
795 in near surface air at Cape Grim, 2005-2006 – I E Galbally, C P Meyer, S T Bentley,  
796 *Baseline Atmospheric Program Australia 2005-2006*, 77-79, 2007.

797 Giglio, L., Randerson, J. T., and van der Werf, G. R.: Analysis of daily, monthly, and  
798 annual burned area using the fourth-generation global fire emissions database (GFED4),  
799 *Journal of Geophysical Research: Biogeosciences*, 118, 317-328, 10.1002/jgrg.20042, 2013.

800 Gong, S. L.: A parameterization of sea-salt aerosol source function for sub- and super-  
801 micron particles, *Global Biogeochem Cy*, 17, Artn 1097 Doi 10.1029/2003gb002079, 2003.

802 Gras, J. L.: Particles Program Report, *Baseline Atmospheric Program Australia 2005-*  
803 *2006*, 85-86, 2007.

804 Goodrick, S. L., Achtemeier, G. L., Larkin, N. K., Liu, Y., and Strand, T. M.: Modelling  
805 smoke transport from wildland fires: a review, *International Journal of Wildland Fire*,  
806 22, 83, 10.1071/wf11116, 2013.

807 Hecobian, A., Liu, Z., Hennigan, C. J., Huey, L. G., Jimenez, J. L., Cubison, M. J., Vay,  
808 S., Diskin, G. S., Sachse, G. W., Wisthaler, A., Mikoviny, T., Weinheimer, A. J., Liao, J.,  
809 Knapp, D. J., Wennberg, P. O., Kurten, A., Crouse, J. D., St Clair, J., Wang, Y., and  
810 Weber, R. J.: Comparison of chemical characteristics of 495 biomass burning plumes  
811 intercepted by the NASA DC-8 aircraft during the ARCTAS/CARB-2008 field campaign,  
812 *Atmospheric Chemistry and Physics*, 11, 13325-13337, 10.5194/acp-11-13325-2011, 2012.

813 Hess, G. D.: A photochemical model for air quality assessment: Model description and  
814 verification, *Atmospheric Environment* (1967), 23, 643-660,  
815 [http://dx.doi.org/10.1016/0004-6981\(89\)90013-9](http://dx.doi.org/10.1016/0004-6981(89)90013-9), 1989.

816 Hurley, P.: Development and Verification of TAPM, in: *Air Pollution Modeling and Its*  
817 *Application XIX*, edited by: Borrego, C., and Miranda, A. I., Springer Netherlands,  
818 Dordrecht, 208-216, 2008a.

819 Hurley, P. J.: TAPM V4. Part 1. Technical description, *CSIRO Marine and Atmospheric*  
820 *Research Internal Report*, 2008b.

821 Jaffe, D. A., and Wigder, N. L.: Ozone production from wildfires: A critical review,  
822 *Atmospheric Environment*, 51, 1-10, 10.1016/j.atmosenv.2011.11.063, 2012.

823 Jost, C., Trentmann, J., Sprung, D., Andreae, M. O., McQuaid, J. B., and Barjat, H.:  
824 Trace gas chemistry in a young biomass burning plume over Namibia: Observations and  
825 model simulations, *Journal of Geophysical Research-Atmospheres*, 108, 13, 8482  
826 10.1029/2002jd002431, 2003.

827 Kaiser, J. W., Heil, A., Andreae, M. O., Benedetti, A., Chubarova, N., Jones, L.,  
828 Morcrette, J. J., Razinger, M., Schultz, M. G., Suttie, M., and van der Werf, G. R.:

829 **Biomass burning emissions estimated with a global fire assimilation system based on**  
830 **observed fire radiative power, *Biogeosciences*, 9, 527-554, 10.5194/bg-9-527-2012, 2012.**

831 **Keywood, M., Guyes, H., Selleck, P., and Gillett, R.: Quantification of secondary organic**  
832 **aerosol in an Australian urban location, *Environmental Chemistry*, 8, 115-126,**  
833 **10.1071/en10100, 2011a.**

834 **Keywood, M., Kanakidou, M., Stohl, A., Dentener, F., Grassi, G., Meyer, C. P., Torseth,**  
835 **K., Edwards, D., Thompson, A., Lohmann, U., and Burrows, J. P.: Fire in the Air-**  
836 **Biomass burning impacts in a changing climate, *Critical Reviews in Environmental***  
837 **Science and Technology, DOI:10.1080/10643389.2011.6042482011b.**

838 **Keywood, M., Cope, M., Meyer, C. P. M., Iinuma, Y., and Emmerson, K.: When smoke**  
839 **comes to town: The impact of biomass burning smoke on air quality, *Atmospheric***  
840 **Environment**, 121, 13-21, <http://dx.doi.org/10.1016/j.atmosenv.2015.03.050>, 2015.

841 **Korontzi, S., Ward, D. E., Susott, R. A., Yokelson, R. J., Justice, C. O., Hobbs, P. V.,**  
842 **Smithwick, E. A. H., and Hao, W. M.: Seasonal variation and ecosystem dependence of**  
843 **emission factors for selected trace gases and PM<sub>2.5</sub> for southern African savanna fires,**  
844 ***Journal of Geophysical Research: Atmospheres*, 108, n/a-n/a, 10.1029/2003JD003730,**  
845 **2003.**

846 **Krummel, P. B., Fraser, P., Steele, L. P., Porter, L. W., Derek, N., Rickard, C., Dunse, B.**  
847 **L., Langenfelds, R. L., Miller, B. R., Baly, S. B., and McEwan, S.: The AGAGE in situ**  
848 **program for non-CO<sub>2</sub> greenhouse gases at Cape Grim, 2005-2006: methane, nitrous**  
849 **oxide, carbon monoxide, hydrogen, CFCs, HCFCs, HFCs, PFCs, halons, chlorocarbons,**  
850 **hydrocarbons and sulphur hexafluoride, *Baseline Atmospheric Program Australia 2005-***  
851 **2006, 2007.**

852 **Lawson, S. J., Keywood, M. D., Galbally, I. E., Gras, J. L., Cainey, J. M., Cope, M. E.,**  
853 **Krummel, P. B., Fraser, P. J., Steele, L. P., Bentley, S. T., Meyer, C. P., Ristovski, Z., and**  
854 **Goldstein, A. H.: Biomass burning emissions of trace gases and particles in marine air at**  
855 **Cape Grim, Tasmania, *Atmos. Chem. Phys.*, 15, 13393-13411, 10.5194/acp-15-13393-**  
856 **2015, 2015.**

857 **Lei, W., Li, G., and Molina, L. T.: Modeling the impacts of biomass burning on air quality**  
858 **in and around Mexico City, *Atmospheric Chemistry and Physics*, 13, 2299-2319,**  
859 **10.5194/acp-13-2299-2013, 2013.**

860 **Lu, H., and Shao, Y. P.: A new model for dust emission by saltation bombardment, *J***  
861 ***Geophys Res-Atmos*, 104, 16827-16841, Doi 10.1029/1999jd900169, 1999.**

862 **Luhar, A. K., Mitchell, R. M., Meyer, C. P., Qin, Y., Campbell, S., Gras, J. L., and Parry,**  
863 **D.: Biomass burning emissions over northern Australia constrained by aerosol**  
864 **measurements: II—Model validation, and impacts on air quality and radiative forcing,**  
865 ***Atmospheric Environment*, 42, 1647-1664,**  
866 **<http://dx.doi.org/10.1016/j.atmosenv.2007.12.040>, 2008.**

867 **Mason, S. A., Trentmann, J., Winterrath, T., Yokelson, R. J., Christian, T. J., Carlson,**  
868 **L. J., Warner, T. R., Wolfe, L. C., and Andreae, M. O.: Intercomparison of Two Box**  
869 **Models of the Chemical Evolution in Biomass-Burning Smoke Plumes, *Journal of***  
870 ***Atmospheric Chemistry*, 55, 273-297, 10.1007/s10874-006-9039-5, 2006.**

871 **McGregor, J. L.: Recent developments in variable-resolution global climate modelling,**  
872 ***Climatic Change*, 129, 369-380, 10.1007/s10584-013-0866-5, 2015.**

873 Meyer, C. P., Luhar, A. K., and Mitchell, R. M.: Biomass burning emissions over  
874 northern Australia constrained by aerosol measurements: I—Modelling the distribution  
875 of hourly emissions, *Atmospheric Environment*, 42, 1629-1646,  
876 <http://dx.doi.org/10.1016/j.atmosenv.2007.10.089>, 2008.

877 Ortega, A. M., Day, D. A., Cubison, M. J., Brune, W. H., Bon, D., de Gouw, J. A., and  
878 Jimenez, J. L.: Secondary organic aerosol formation and primary organic aerosol  
879 oxidation from biomass-burning smoke in a flow reactor during FLAME-3, *Atmospheric  
880 Chemistry and Physics*, 13, 11551-11571, 10.5194/acp-13-11551-2013, 2013.

881 Pacifico, F., Folberth, G. A., Sitch, S., Haywood, J. M., Rizzo, L. V., Malavelle, F. F., and  
882 Artaxo, P.: Biomass burning related ozone damage on vegetation over the Amazon forest:  
883 a model sensitivity study, *Atmos. Chem. Phys.*, 15, 2791-2804, 10.5194/acp-15-2791-2015,  
884 2015.

885 Parrington, M., Palmer, P. I., Henze, D. K., Tarasick, D. W., Hyer, E. J., Owen, R. C.,  
886 Helmig, D., Clerbaux, C., Bowman, K. W., Deeter, M. N., Barratt, E. M., Coheur, P. F.,  
887 Hurtmans, D., Jiang, Z., George, M., and Worden, J. R.: The influence of boreal biomass  
888 burning emissions on the distribution of tropospheric ozone over North America and the  
889 North Atlantic during 2010, *Atmospheric Chemistry and Physics*, 12, 2077-2098,  
890 10.5194/acp-12-2077-2012, 2012.

891 Paugam, R., Wooster, M., Freitas, S., and Val Martin, M.: A review of approaches to  
892 estimate wildfire plume injection height within large-scale atmospheric chemical  
893 transport models, *Atmos. Chem. Phys.*, 16, 907-925, 10.5194/acp-16-907-2016, 2016.

894 Reid, C. E., Brauer, M., Johnston, F. H., Jerrett, M., Balmes, J. R., and Elliott, C. T.:  
895 Critical Review of Health Impacts of Wildfire Smoke Exposure, *Environmental health  
896 perspectives*, 124, 1334-1343, 10.1289/ehp.1409277, 2016.

897 Reid, J. S., Hyer, E. J., Prins, E. M., Westphal, D. L., Zhang, J., Wang, J., Christopher,  
898 S. A., Curtis, C. A., Schmidt, C. C., Eleuterio, D. P., Richardson, K. A., and Hoffman, J.  
899 P.: Global Monitoring and Forecasting of Biomass-Burning Smoke: Description of and  
900 Lessons From the Fire Locating and Modeling of Burning Emissions (FLAMBE)  
901 Program, *IEEE Journal of Selected Topics in Applied Earth Observations and Remote  
902 Sensing*, 2, 144-162, 10.1109/JSTARS.2009.2027443, 2009.

903 Reisen, F., Meyer, C. P., McCaw, L., Powell, J. C., Tolhurst, K., Keywood, M. D., and  
904 Gras, J. L.: Impact of smoke from biomass burning on air quality in rural communities  
905 in southern Australia, *Atmospheric Environment*, 45, 3944-3953,  
906 10.1016/j.atmosenv.2011.04.060, 2011.

907 Reisen, F., Duran, S. M., Flannigan, M., Elliott, C., and Rideout, K.: Wildfire smoke and  
908 public health risk, *International Journal of Wildland Fire*, 24, 1029, 10.1071/wf15034,  
909 2015.

910 Sarwar, G., Luecken, D., Yarwood, G., Whitten, G. Z., and Carter, W. P. L.: Impact of  
911 an updated carbon bond mechanism on predictions from the CMAQ modeling system:  
912 Preliminary assessment, *J Appl Meteorol Clim*, 47, 3-14, Doi 10.1175/2007jamc1393.1,  
913 2008.

914 Sarwar, G., Appel, K. W., Carlton, A. G., Mathur, R., Schere, K., Zhang, R., and Majeed,  
915 M. A.: Impact of a new condensed toluene mechanism on air quality model predictions  
916 in the US, *Geosci Model Dev*, 4, 183-193, DOI 10.5194/gmd-4-183-2011, 2011.

917 Seinfeld, J. H., and Pandis, S. N.: Atmospheric chemistry and physics : from air pollution  
918 to climate change, Wiley, New York, xxvii, 1326 p. pp., 1998.

919 Smagorinsky, J.: General circulation experiments with the primitive equations Monthly  
920 Weather Review, 91, 99-164, doi:10.1175/1520-  
921 0493(1963)091<0099:GCEWTP>2.3.CO;2, 1963.

922 Trentmann, J., Yokelson, R. J., Hobbs, P. V., Winterrath, T., Christian, T. J., Andreae,  
923 M. O., and Mason, S. A.: An analysis of the chemical processes in the smoke plume from  
924 a savanna fire, Journal of Geophysical Research-Atmospheres, 110, 20, D12301  
925 10.1029/2004jd005628, 2005.

926 Tsimpidi, A. P., Karydis, V. A., Zavala, M., Lei, W., Molina, L., Ulbrich, I. M., Jimenez,  
927 J. L., and Pandis, S. N.: Evaluation of the volatility basis-set approach for the simulation  
928 of organic aerosol formation in the Mexico City metropolitan area, Atmos Chem Phys,  
929 10, 525-546, 2010.

930 Urbanski, S. P.: Combustion efficiency and emission factors for wildfire-season fires in  
931 mixed conifer forests of the northern Rocky Mountains, US, Atmos. Chem. Phys., 13,  
932 7241-7262, 10.5194/acp-13-7241-2013, 2013.

933 van Leeuwen, T. T., and van der Werf, G. R.: Spatial and temporal variability in the ratio  
934 of trace gases emitted from biomass burning, Atmospheric Chemistry and Physics, 11,  
935 3611-3629, 10.5194/acp-11-3611-2011, 2011.

936 van Leeuwen, T. T., Peters, W., Krol, M. C., and van der Werf, G. R.: Dynamic biomass  
937 burning emission factors and their impact on atmospheric CO mixing ratios, Journal of  
938 Geophysical Research-Atmospheres, 118, 6797-6815, 10.1002/jgrd.50478, 2013.

939 Walcek, C. J.: Minor flux adjustment near mixing ratio extremes for simplified yet highly  
940 accurate monotonic calculation of tracer advection, Journal of Geophysical Research:  
941 Atmospheres, 105, 9335-9348, 10.1029/1999JD901142, 2000.

942 Wigder, N. L., Jaffe, D. A., and Saketa, F. A.: Ozone and particulate matter  
943 enhancements from regional wildfires observed at Mount Bachelor during 2004-2011,  
944 Atmospheric Environment, 75, 24-31, 10.1016/j.atmosenv.2013.04.026, 2013.

945 Yokelson, R. J., Bertschi, I. T., Christian, T. J., Hobbs, P. V., Ward, D. E., and Hao, W.  
946 M.: Trace gas measurements in nascent, aged, and cloud-processed smoke from African  
947 savanna fires by airborne Fourier transform infrared spectroscopy (AFTIR), Journal of  
948 Geophysical Research-Atmospheres, 108, 8478 10.1029/2002jd002322, 2003.

949 Yokelson, R. J., Karl, T., Artaxo, P., Blake, D. R., Christian, T. J., Griffith, D. W. T.,  
950 Guenther, A., and Hao, W. M.: The Tropical Forest and Fire Emissions Experiment:  
951 overview and airborne fire emission factor measurements, Atmospheric Chemistry and  
952 Physics, 7, 5175-5196, 2007.

953 Yokelson, R. J., Crouse, J. D., DeCarlo, P. F., Karl, T., Urbanski, S., Atlas, E., Campos,  
954 T., Shinzuka, Y., Kapustin, V., Clarke, A. D., Weinheimer, A., Knapp, D. J., Montzka,  
955 D. D., Holloway, J., Weibring, P., Flocke, F., Zheng, W., Toohey, D., Wennberg, P. O.,  
956 Wiedinmyer, C., Mauldin, L., Fried, A., Richter, D., Walega, J., Jimenez, J. L., Adachi,  
957 K., Buseck, P. R., Hall, S. R., and Shetter, R.: Emissions from biomass burning in the  
958 Yucatan, Atmospheric Chemistry and Physics, 9, 5785-5812, 2009.

959 Yokelson, R. J., Burling, I. R., Urbanski, S. P., Atlas, E. L., Adachi, K., Buseck, P. R.,  
960 Wiedinmyer, C., Akagi, S. K., Toohey, D. W., and Wold, C. E.: Trace gas and particle

961 **emissions from open biomass burning in Mexico, Atmospheric Chemistry and Physics,**  
962 **11, 6787-6808, 10.5194/acp-11-6787-2011, 2011.**  
963

964

965 **Table 1. EF used in model sensitivity studies, corresponding to low (MCE=0.89), medium (MCE=0.92) and**  
 966 **high (MCE = 0.95) MCEs. A subset of the total species included in the CB05 lumped chemical mechanism**  
 967 **are shown. Also shown are savannah EF from Andreae and Merlet (2001) (A&M) and EF calculated from**  
 968 **BB2 in previous work (Lawson et al., 2015). NO = nitric oxide, CO =carbon monoxide, PAR=paraffin**  
 969 **carbon bond, OLE= terminal olefin carbon bond, TOL=toluene and other monoalkyl aromatics,**  
 970 **XYL=xylene and other polyalkyl aromatics, BNZ =benzene, FORM=formaldehyde, ALD2=acetaldehyde,**  
 971 **EC=elemental carbon <10  $\mu\text{m}$ , OC=primary organic carbon < 10  $\mu\text{m}$**

972

973

974

	EF g kg <sup>-1</sup>				
	A&M (2001) MCE 0.94	Lawson et al., (2015) MCE 0.88	Used in this work		
			MCE 0.89	MCE 0.92	MCE 0.95
NO	3.9	n/a	0.8	2.7	4.7
CO	65	127	121	89	57
PAR	1.55	n/a	2.33	2.02	1.40
OLE	0.54	n/a	0.81	0.7	0.49
TOL	0.2	0.30	0.3	0.26	0.18
XYL	0.045	0.26	0.07	0.06	0.04
BNZ	0.23	0.69	0.35	0.3	0.21
FORM	0.42	1.64	0.63	0.55	0.38
ALD2	0.5	0.92	0.75	0.65	0.45
EC	0.48	0.16	0.19	0.34	0.53
OC	3.40	n/a	5.10	4.08	3.06
NMOC/NO <sub>x</sub>	1.60	n/a	11.99	2.97	1.20

975

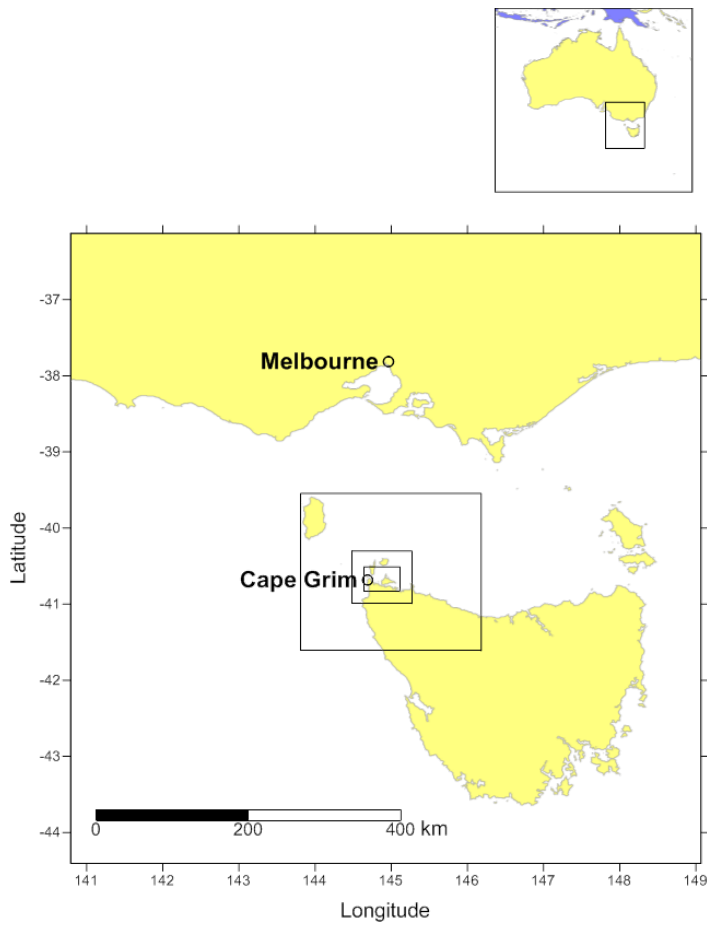
1 **Table 2. Summary of sensitivity study results, including Meteorology, Emission Factors and Spatial**  
 2 **Variability.**

3

4

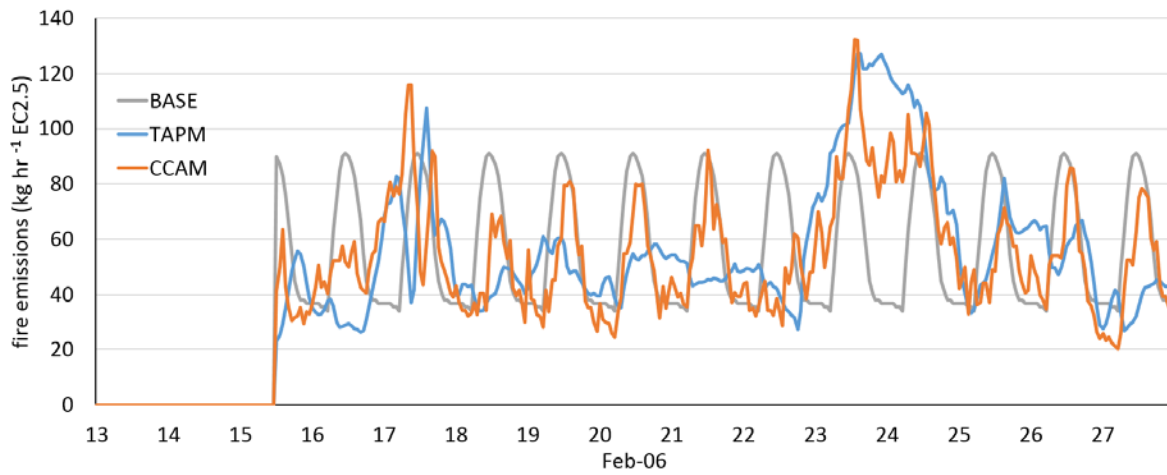
Sensitivity study	Species	TAPM-CTM simulation	CCAM-CTM simulation	Comments/drivers of model outputs
Meteorology (Section 3.1.1)	BC and CO	BB1 plume strike +3 hr Duration 12 hr (actual 5 hr)	BB1 plume strike -12 hr Duration 36 hr intermittent (actual 5 hr)	Narrow BB plume. Differences in plume strike due to timing of wind direction change; windspeeds; direct or indirect advection of plume over Cape Grim
		BB2 plume strike -26 hr Duration 50 hr (actual 29 hr)	BB2 plume strike -26 hr Duration 57 hr (actual 29 hr)	Wind direction differences driven by gravity wave oscillations; timing of wind direction change; different wind speeds driving absolute BB emissions and plume dispersion
	O <sub>3</sub>	4 O <sub>3</sub> peaks simulated (2 observed, 2 not)	1 O <sub>3</sub> peak simulated (observed)	Differences in simulated wind speed and direction (and EF – see below)
Emission Factors (Section 3.1.2)	BC and CO	BC peak magnitude varies by factor 3, CO factor 2 with different EF runs	As for TAPM -CTM	Concentrations vary according to EF input ratios.
	O <sub>3</sub>	2 peaks with high EF sensitivity, 2 peaks with no EF sensitivity	1 peak with no EF sensitivity	Different NMOC/NO <sub>x</sub> emission ratios (varies with MCE) drives destruction or production of O <sub>3</sub> in fire related peaks. MCE 0.89 TAPM-CTM simulation gives best agreement with observations
Spatial Variability (Section 3.1.3)	CO	Differences of up to > 500 ppb in grid points 1 km apart (BB2)	n/a	Narrow BB plume
	O <sub>3</sub>	Differences of up to 15 ppb in grid points 1 km apart (BB1)	n/a	Narrow ozone plume generated downwind of fire

5



6

7 **Figure 1. The five nested computational domains used in TAPM-CTM and CCAM-CTM, showing cell**  
 8 **spacings of 20 km, 12 km, 3 km, 1 km and 400 m.**



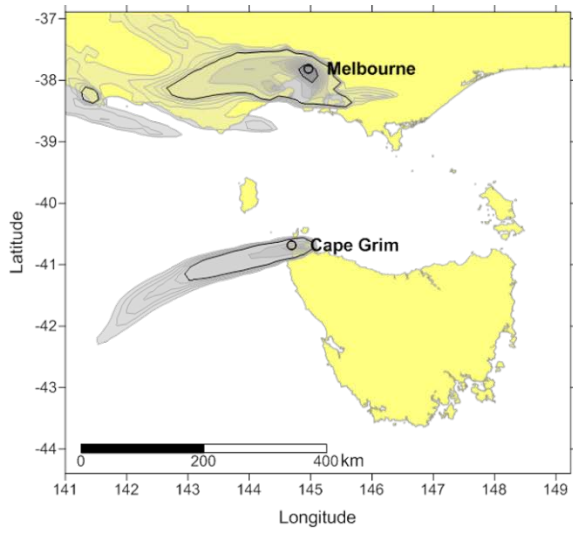
9

10 **Figure 2 Base hourly diurnal emissions and revised Macarthur Fire Danger Index (FDI)-scale emissions**  
 11 **generated using TAPM and CCAM meteorology.**

12

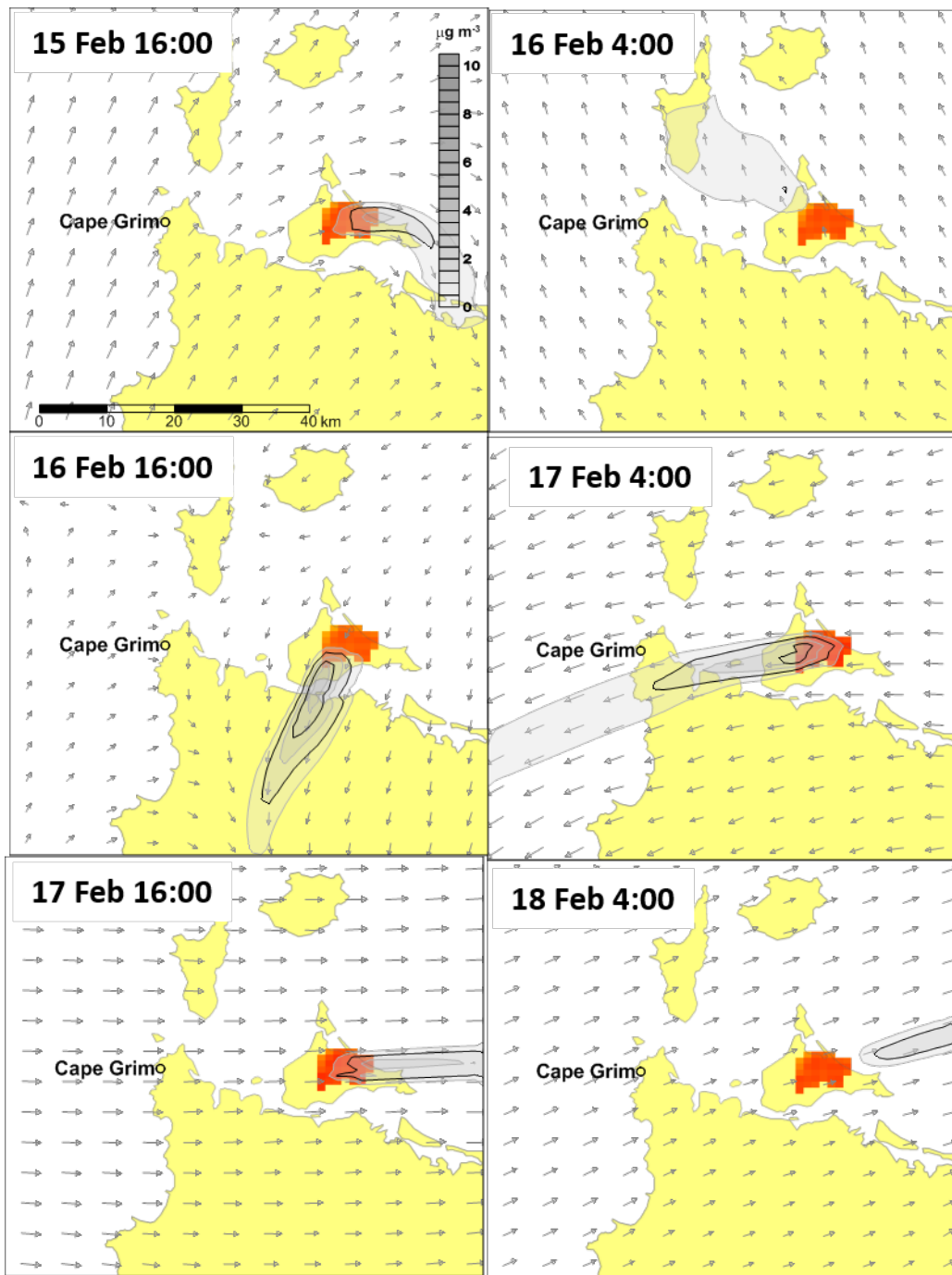


13



14

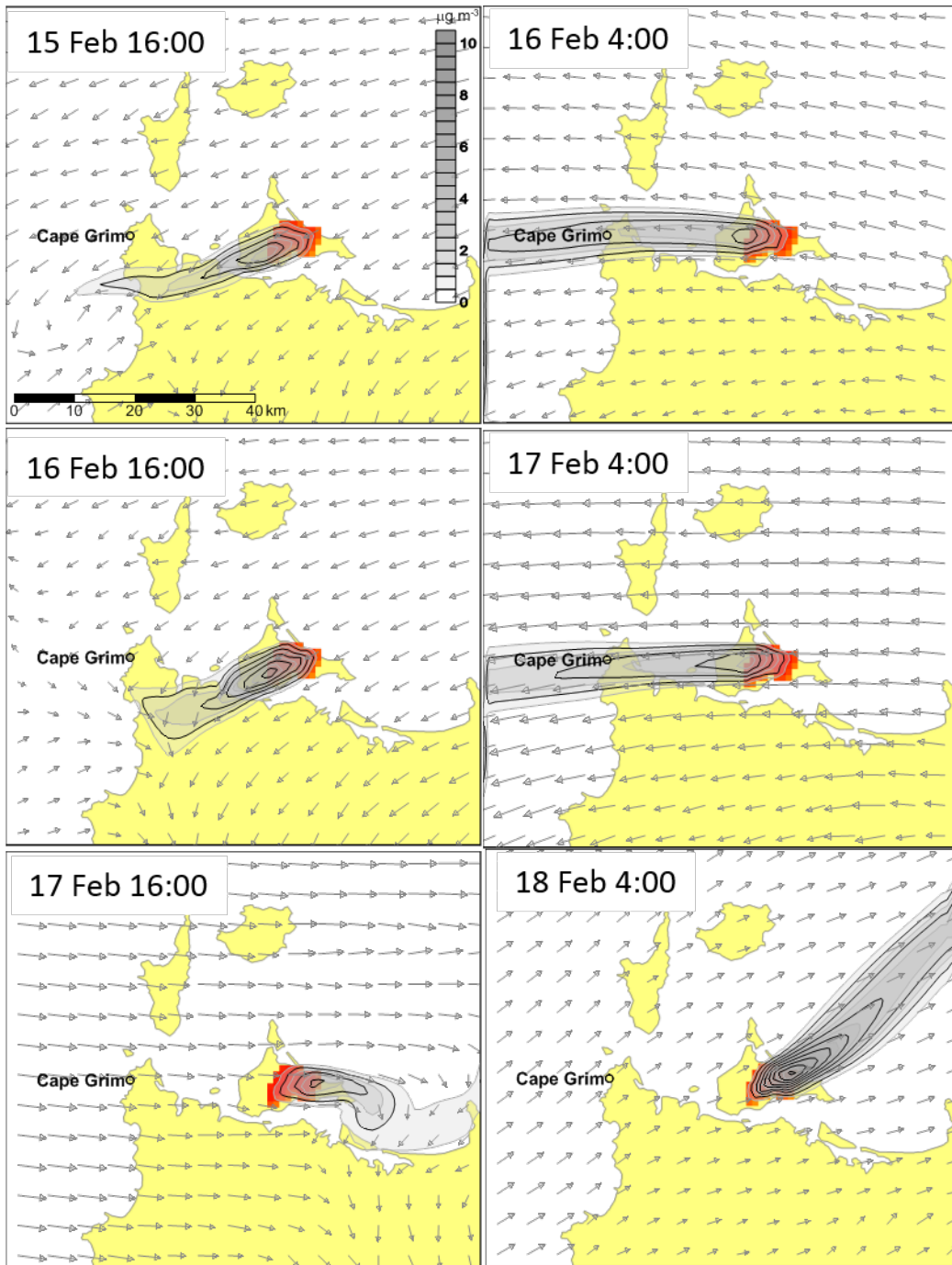
15 **Figure 3. Model output of BC (left) on the 23rd February, with a MODIS Truecolour image of the same**  
16 **period.**



17

18 **Figure 4. Model output of BC for TAPM-CTM at 12 hour time intervals during BB1, showing the Robbins**  
 19 **Island BB plume intermittently striking Cape Grim, and then the change in plume direction with wind**  
 20 **direction change. Arrows are wind vectors.**

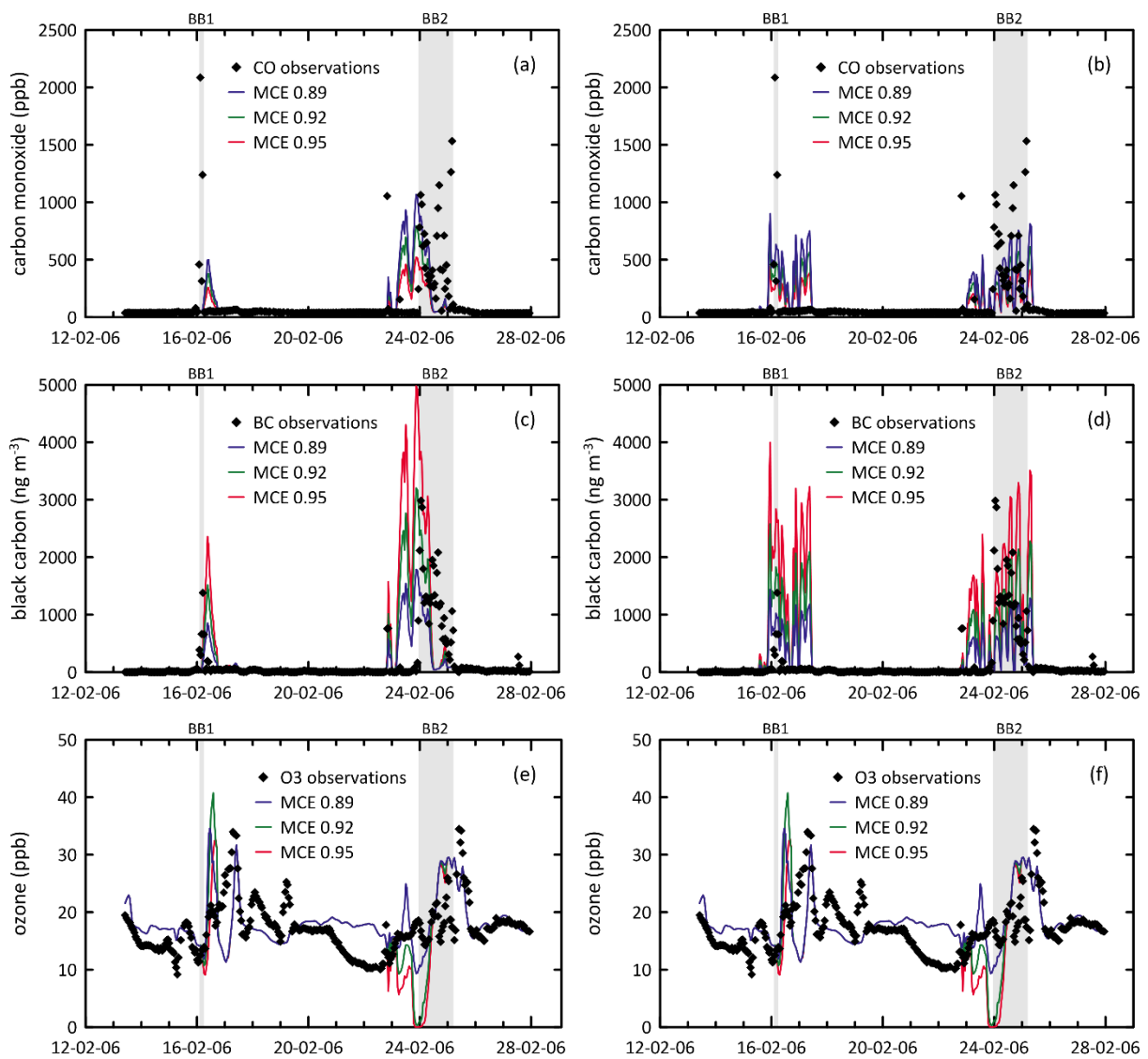
21



22

23 **Figure 5. Model output of BC for CCAM-CTM at 12 hour time intervals during BB1, showing the Robbins**  
 24 **Island BB plume intermittently striking Cape Grim, and then the change in plume direction with wind**  
 25 **direction change. Arrows are wind vectors.**

26



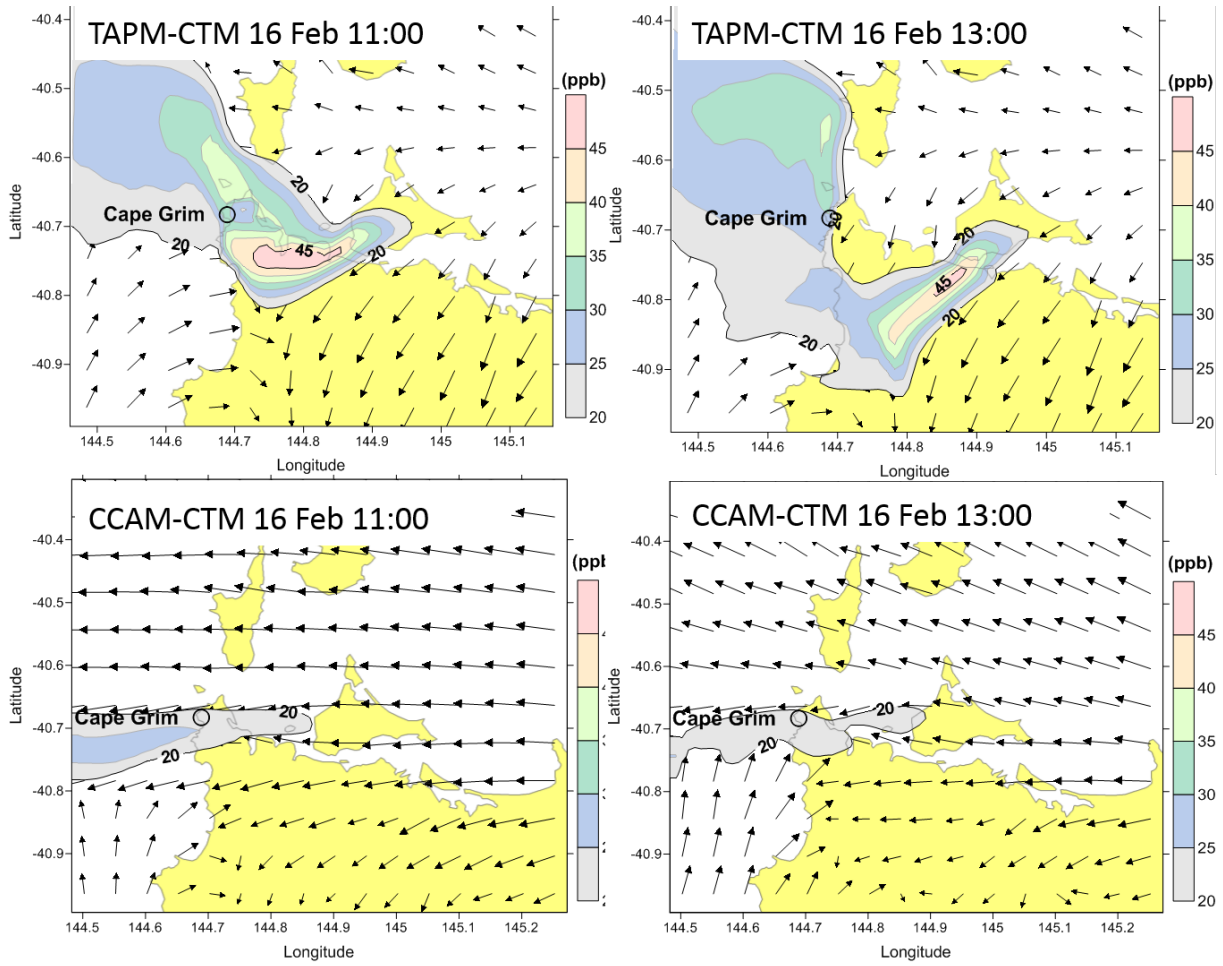
27

28 **Figure 6. Simulated CO using a) TAPM-CTM and b) CCAM-CTM, simulated BC using c) TAPM-CTM**  
 29 **and d) CCAM-CTM, and simulated O<sub>3</sub> using e) TAPM-CTM and f) CCAM-CTM. Coloured lines represent**  
 30 **different MCE EF simulations, black symbols are observations**

31

32

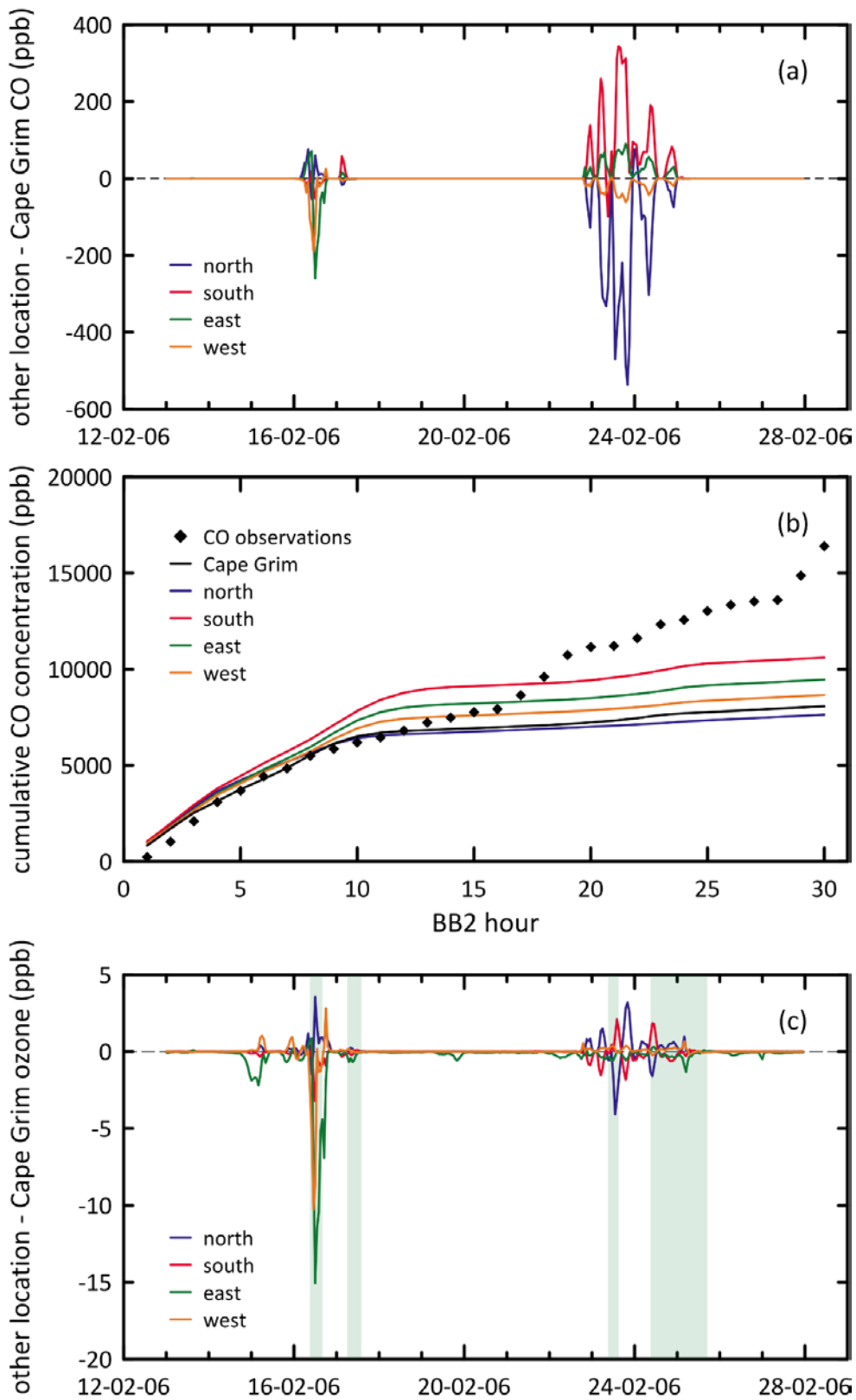
33



34

35 **Figure 7 Model output showing O<sub>3</sub> enhancement downwind of the fire during BB1 at 11:00 and 13:00 on**  
36 **the 16 February for TAPM-CTM (top) and CCAM-CTM (bottom). The spatially variable plume and**  
37 **complex wind fields are shown. Arrows are wind vectors.**

38



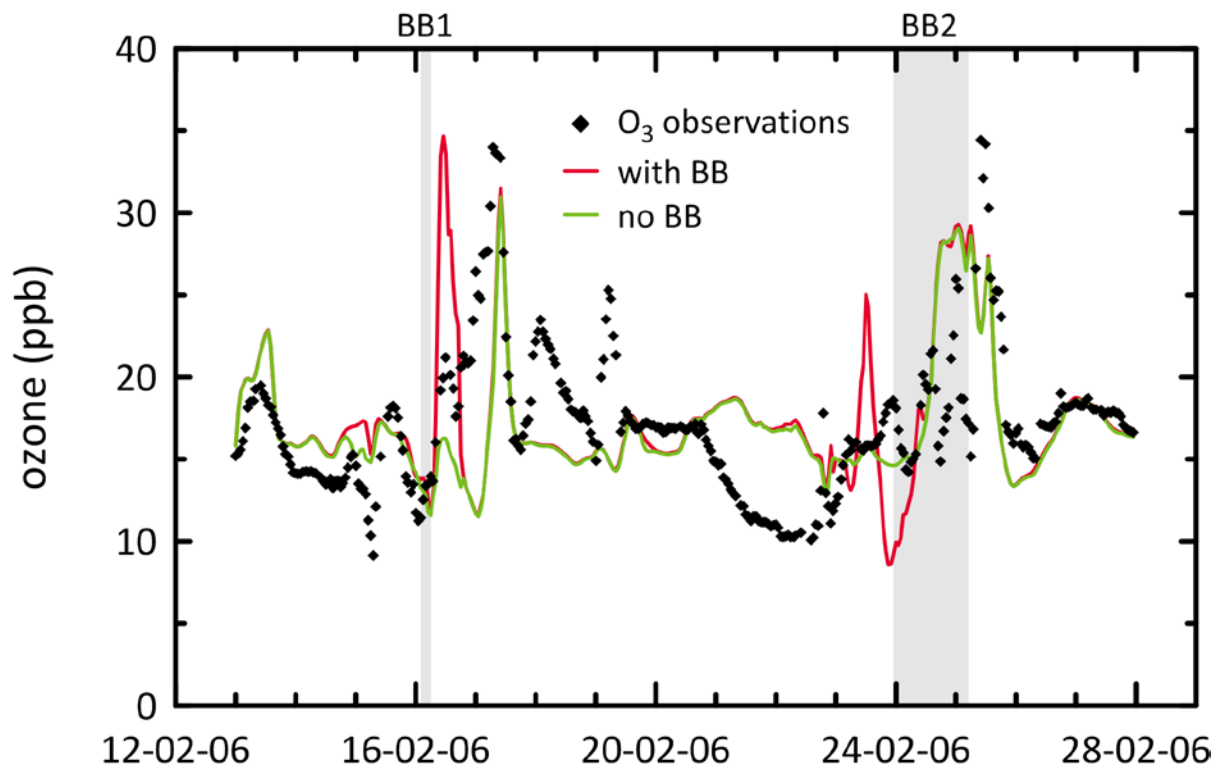
39

40 **Figure 8 Simulated spatial variability using TAPM-CTM with MCE=0.89 showing a) time series of CO**  
 41 **over two weeks of fire (BB1 and BB2 shown), b) the observed and modelled cumulative concentration of**  
 42 **CO over the 29 hour duration of BB2 and c) time series of O<sub>3</sub> over the two weeks of fire. The four modelled**  
 43 **O<sub>3</sub> peaks in the Cape Grim gridpoint are shaded. Figs a and c show the difference between simulated**

44 concentrations at Cape Grim and at 4 surrounding grid points 1km north, south, east and west of Cape  
45 Grim. Fig b shows simulated cumulative CO at Cape Grim and at 4 surrounding grid points. . Observations  
46 are black symbols.

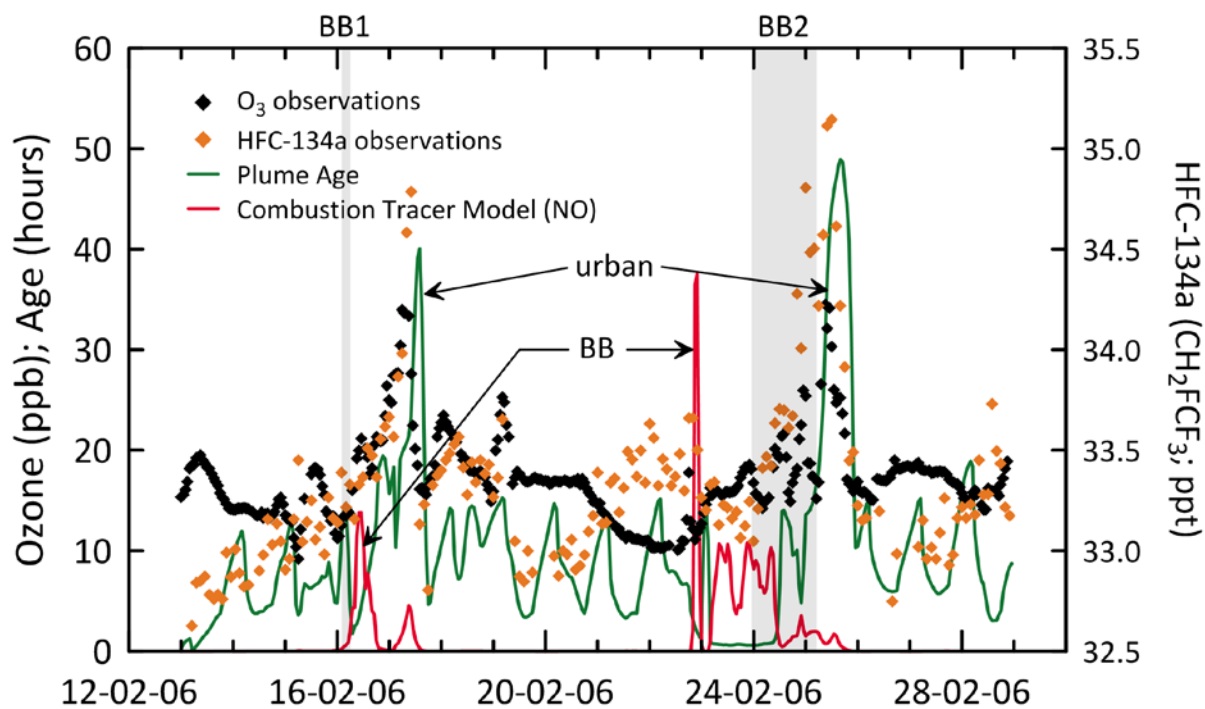
47

48



49

50 Figure 9 Simulated O<sub>3</sub> concentration at Cape Grim with the Robbins Island fire emissions (red line) and  
51 without the fire emissions (green line). Observations are black symbols. Model used was TAPM-CTM with  
52 EF corresponding to MCE=0.89. The periods corresponding to observed BB1 and BB2 are shaded.



53  
 54 **Figure 10 Simulated plume age (green line), simulated combustion tracer (NO) (red line), observed O<sub>3</sub>**  
 55 **(black symbols) and observed HFC-134a (orange symbols) over 2 week duration of the fire. The modelled**  
 56 **BB periods (red peaks) and impact of urban air from mainland Australia (green peaks) are labelled. The**  
 57 **periods corresponding to observed BB1 and BB2 are shaded.**

58

59

60

61

62 End